Macromolecules

pubs.acs.org/Macromolecules Article

Extensional Viscosity of Immiscible Polymer Multi-Nanolayer Films: Signature of the Interphase

Anna Dmochowska, Jorge Peixinho,* Cyrille Sollogoub, and Guillaume Miquelard-Garnier*

Cite This: *Macromolecules* 2023, 56, 6222−6231 Read Online

ACCESS | Metrics & More | Article Recommendations | Supporting Information

ABSTRACT: The measurement of interfacial mechanical or rheological properties in polymer blends is a challenging task, as well as providing a quantitative link between these properties and the interfacial nanostructure. Here, we perform a systematic study of the extensional rheology of multilayer films of an immiscible polymer pair, polystyrene and poly(methyl methacrylate). We take advantage of multi-nanolayer coextrusion to increase the number of interfaces up to thousands, consequently magnifying the interfacial response of the films. The transient elongational response is compared to an additivity rule model based on the summation of the contribution of each polymer as well as the interfacial one. At low strain rates, the model reproduces the transient extensional viscosity up to strain-thinning, while at larger strain rates, the extra stress exceeds the prediction based on constant interfacial tension. This extra contribution is attributed to an interphase modulus on the order of 1−10 MPa, which increases with the strain rate following a power law with an exponent of 1/3. The extensional rheology of multi-nanolayer films is then an efficient combination to go beyond interfacial tension and quantitatively measure the interfacial rheology of immiscible polymer blends.

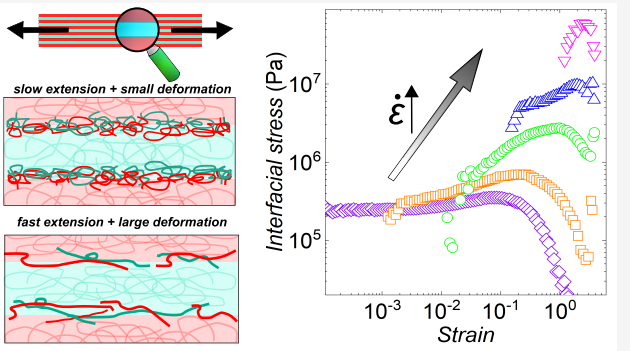

INTRODUCTION

Polymer blends represent today more than a third of the world's plastic production, despite the fact that most polymers are immiscible,[1] which results in phase separation and unentangled interfaces. To circumvent these phenomena, compatibilization has been mastered for a long time industrially to achieve suitable properties for such immiscible blends. It consists of modifying the interface with several possible strategies, such as the addition or the in situ formation of a copolymer[2] that will segregate at the interface, resulting in a more diffused interface that allows entanglements similar to what is occurring at short times in miscible systems,[3,4] the use of nanoparticles[5−7] and cosolvents,[8] or through ionic bonds[9] and electrostatic correlations.[10]

The effect of the compatibilizer, such as the role of molecular weight or the amount of copolymer, has been quantified long ago on interfacial properties in the solid-state-like fracture toughness at the interface.[11,12] However, it was only recently that the complex viscosity of a compatibilized interface has been characterized over a large frequency range.[13,14] To do so, we took advantage of multi-nanolayer coextrusion that applies successive slicing and recombining a stratified polymer melt flow, giving rise to a material made of thousands of alternating nanometric layers.[15,16] By doing so, the effect of interfaces was drastically enhanced in the response of the materials under oscillatory shear. In noncompatibilized blends, a quantitative link has also been established between the fracture toughness and, this time, the interfacial nanometric thickness, which depends on the Flory−Huggins interaction parameter between the two polymers.[17] Similarly, in the melt, a relation between viscoelastic moduli and interfacial tension has been proposed[18,19] and used to describe the melt properties of polymer blends. Still, measuring interfacial tension of immiscible polymers is a tedious task[20,21] due to the high viscosities and temperatures involved and does not always provide sufficient information for designing and processing optimized nanostructured blends;[22] even in simple mixtures, flows may be impacted by surface tension gradients (the well-known Marangoni effect). Hence, a full characterization of the interfacial rheology, i.e., not only the measurement of interfacial tension but also the possible evolution of the interfacial rheological properties in relation to the morphology of the interface and processing parameters, is lacking in the literature.

Extensional rheology is a challenging but rapidly developing technique to measure elongational flows, which allowed, in

Received: February 17, 2023
Revised: June 22, 2023
Published: August 11, 2023

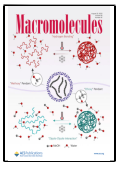

https://doi.org/10.1021/acs.macromol.3c00288
Macromolecules 2023, 56, 6222−6231

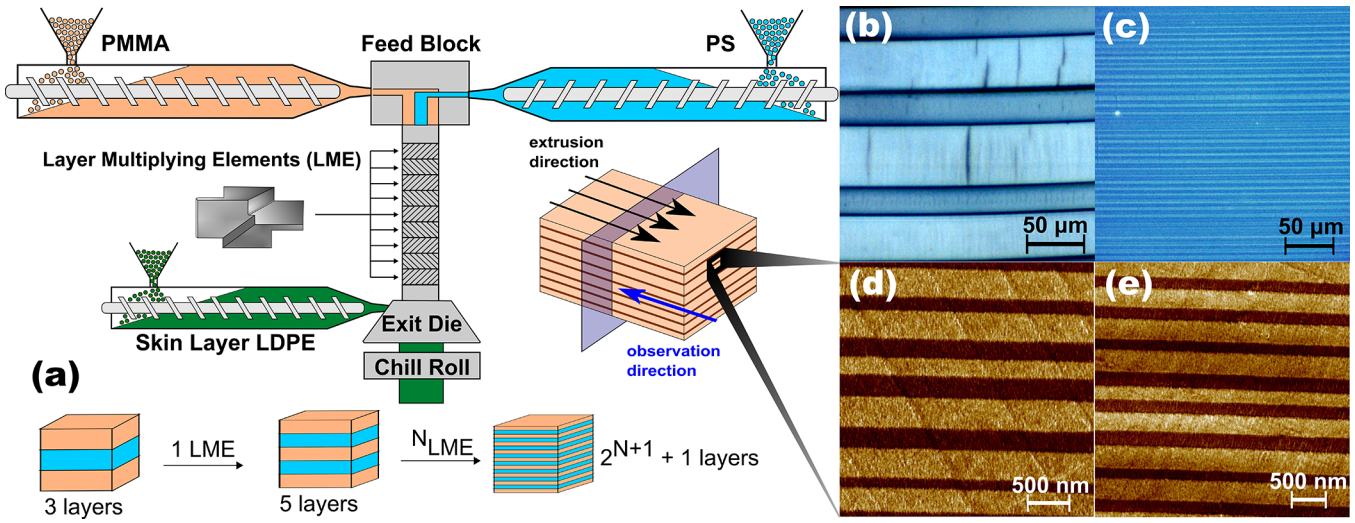

Figure 1. Multi-nanolayer coextrusion scheme (a) with typical images of fabricated films: (b) 17 layers (the black vertical strokes are compression lines present due to cutting); (c) 129 layers; (d) 2049 layers; and (e) 4097 layers. On images from the optical microscope (b, c), the lighter blue corresponds to PS and the darker blue corresponds to PMMA. On AFM images (d, e), the color gold represents PS layers, while brown represents PMMA layers.

particular, to reexamine fundamental theories in polymer physics, such as the tube model.[23,24] In this study, we aim to take advantage of this technique applied to multi-nanolayer films of a well-known polymer couple, polystyrene (PS) and poly(methyl methacrylate) (PMMA), in order to study the flow properties of their interface. Extensional rheology of PS[25,26] and PMMA[27,28] has already been investigated separately. The effect of molecular weight, a rise of transient extensional viscosity above the predictions from linear viscoelasticity theory, and strain hardening have been well-documented for both polymers. However, there have been only a few reports of the extensional rheometry of multilayer films. Notably, Lamnawar et al. have studied the dynamics of interdiffusion across the interfaces during processing of a miscible polymer pair,[29−32] as well as the in situ compatibilization reaction of an immiscible one.[33] Levitt et al.[34] first related the stretching of multilayer films to interfacial tension. Later, in the same group, Jordan et al.[35] implemented a model using an additivity rule, i.e., a viscosity that is the arithmetic average of the viscosity with respect to the volume fraction of each polymer, complemented with an interfacial tension contribution to reproduce the tensile stress growth of various polymer pairs. Building on this approach, we propose here a systematic study of the transient extensional stress of PS/PMMA multi-nanolayer films, where the number of interfaces varies from 2 to 4096 and the strain rates from 0.001 to 10 s^{-1}, hence from quasi-static to nonlinear flow. Such a high number of interfaces results in a drastic increase of interfacial contribution to the rheological response of the films. This, in turn, allows the direct measurement of the extensional viscosity of the interface and its comparison with theoretical predictions. A large increase of the measured interfacial stress at high strain, dependent on the strain rate, is evidenced for the first time in polymer blends and is reminiscent of the surface elasticity in soap films.

MATERIALS AND METHODS

Materials. Polystyrene PS 1340 from TotalEnergies and poly(methyl methacrylate) PMMA VM100 from Arkema were selected to produce multilayer films based on an earlier work.[36] The molecular weights, glass transition temperatures, and densities have been determined previously.[36,37] The polymers were chosen so that at the coextrusion temperature, a viscosity ratio close to 1 is achieved in the range of shear rates applied during coextrusion (Figure S1). The viscoelastic properties of the neat polymers have been obtained by small-amplitude oscillatory shear (SAOS) measurements at several temperatures ranging from 130 to 225 °C with a DHR 20 (TA Instruments) rheometer with a plate−plate geometry (25 mm diameter and 1 mm gap) under air flow and not nitrogen to simulate the coextrusion conditions. Frequency sweep tests were conducted in the range from 0.045 to 628 rad/s with an applied strain of 1%, in the linear viscoelasticity regime, and confirmed a comparable thermorheological behavior of the two polymers (Figure S3c).[26,38] The zero-shear viscosity (η_0) was determined by using a classical Carreau−Yasuda model,[39] similar to our previous work.[40] The main properties of the neat polymers are listed in Table S1.

Film Fabrication. PS/PMMA films were produced by using a lab-made customized multilayer coextrusion line[41] schematized in Figure 1. It consists of three 20 mm single-screw Rheoscam extruders (Scamex), two melt-gear pumps, a three-layer feed block, layer-multiplying elements (LME), a flat die, and a chill roll. The temperature of the PS and PMMA extruders, feed block, and LME assembly was set to 225 °C. The composition could be controlled by tuning the screw speed and controlling the gear pumps. The melted polymers enter through a three-layer feed block connected to a channel of constant height with a series of LMEs, where the flow for each LME is first split vertically and then spread horizontally and recombined. An assembly of N LMEs results in a film composed of $n = 2^{N+1} + 1$ layers. In this study, films with 3, 17, 129, 2049, and 4097 layers were obtained with 0, 3, 6, 10, and 11 LMEs, respectively. After exiting the last LME, the polymer melt enters a flat exit die with a 2 mm gap and 150 mm width with the temperature set to 200 °C. Finally, the film is collected using a chill roll heated up to 90 °C with the lowest possible drawing speed to prevent post-extrusion chain relaxation, which would lead to shrinking of the samples when reheated above glass transition temperature during the extensional rheology measurement. Additionally, to reduce the thickness of the final film without any post-stretching step, a sacrificial layer of low-density polyethylene, LDPE 1022 FN (TotalEnergies), is added at the exit die. This sacrificial layer has no adhesion with the multilayer film and is peeled before any measurements.

In this work, the two studied weight compositions of PS/PMMA multilayer films are close to 60/40 and 30/70 and have thicknesses (H_M) lower than 1 mm to fulfill the requirements of the extensional

https://doi.org/10.1021/acs.macromol.3c00288
Macromolecules 2023, 56, 6222−6231

rheology measurements. The exact compositions and thicknesses of the extruded films are given in Table S2.

Film Morphology. The morphology and individual layer thicknesses of the films were characterized with an optical microscope Axio Imager 2 (ZEISS) or an atomic force microscope (AFM) Nanoscope V (Veeco), depending on the expected layer thickness. In both cases, the samples were cut from the center of the extruded film parallel to extrusion flow and cross-sectioned perpendicular to their surface by using an ultramicrotome with a diamond knife (Diatome). The thickness of at least 10% of the total number of layers was measured in each film by following the procedure developed by Bironeau et al.[42]

Extensional Rheology. The viscoelastic properties in uniaxial stretching were determined by a rheometer MCR 502 (Anton Paar) equipped with a Sentmanat Extensional Rheometer platform SER-2 (Xpansion Instruments),[43,44] which consists of paired counter-rotating drums coupled to the motor. The material is stretched at a constant rotation speed of the drums, and the force required to stretch it is precisely monitored by the torque of the instrument. When a constant strain rate ($\dot{\varepsilon}$) is applied, the cross-section area (A) of the sample is assumed to decrease exponentially with the measurement time following eqs S2−S4. The extensional viscosity (η_E) is then proportional to the instantaneous stretching force, the instantaneous area of the sample, and the strain rate. The films were cut into rectangular samples with a length (L) of about 20 mm and a width (W) of around 11 mm and tested at 155 °C under an air flow. This temperature was optimized so that no thermal degradation will affect the viscosity of the samples over the experimental time scale (see Figure S2), but also that the shrinking is negligible, while the torque is measurable.[45] Five Hencky strain rates ($\dot{\varepsilon}$) ranging from 0.001 to 10 s^{-1}, directly proportional to the shaft rotation rate, were chosen for the measurements and kept constant over the test time. The films were stretched along the extrusion direction. All measurements were repeated at least 3 times and averaged. The tests were performed until the sample breakage or, depending on which happens first, until a strain value of 3.8 due to the limitation of one drum revolution in the SER system.[46,47]

RESULTS AND DISCUSSION

Film Morphology. The morphology of the fabricated PS/PMMA multilayer films is presented in Figure 1. The averaged thicknesses of individual layers of all films are in good agreement with the calculated values obtained from eq S1, as shown in Table S2 in the Supporting Information.

In all cases, the morphology analysis revealed some heterogeneity in the layer thicknesses, which is not unusual for such samples[42] and can also be amplified by the fact that we used the lowest possible draw ratio. As expected, no broken layers are observed for films with 3, 17, or 129 layers. For all but one film with 2049 and 4097 layers, the amount of broken layers is less than 5%. In one film with 4097 layers and the respective average thicknesses of PS and PMMA equal to 124 and 108 nm, the amount of broken layers is close to 9%. Still, due to the low amount of broken layers, they will be neglected in the following analyses, and we will use the average layer thickness.

Rheological Investigation. *Neat Polymer Melts.* In order to proceed from oscillation to extension, the multimode Maxwell model, eqs 1 and 2, was used to determine the linear viscoelastic (LVE) envelope from small-amplitude oscillatory shear (SAOS) data.[48] The time−temperature superposition of storage (G') and loss (G'') moduli for PS and PMMA was performed at 155 °C, the reference temperature of the extensional rheology experiments (see Figure S3a,b). The calculations were done according to the following equations:

$$G'(\omega) = \sum_{i=1}^{N} g_i \frac{(\omega\tau_i)^2}{1 + (\omega\tau_i)^2} \tag{1}$$

$$G''(\omega) = \sum_{i=1}^{N} g_i \frac{\omega\tau_i}{1 + (\omega\tau_i)^2} \tag{2}$$

where ω is the angular frequency, g_i is the relaxation modulus (in Pa), and τ_i is the time constant (s) for element i up to N = 10. The calculated values are summarized in Table S3 in the Supporting Information.

The extensional viscosity in the LVE regime (η_E) calculated from SAOS measurements was plotted as a function of time (t) according to Trouton's ratio[49,50] by using the previously found values of the relaxation modulus and time constant

$$\eta_E(t) = 3\sum_{i=1}^{N} g_i\tau_i(1 - e^{-(t/\tau_i)}) \tag{3}$$

Figure 2 presents measured extensional viscosity (η_E^+) as a function of time for PS and PMMA at different constant

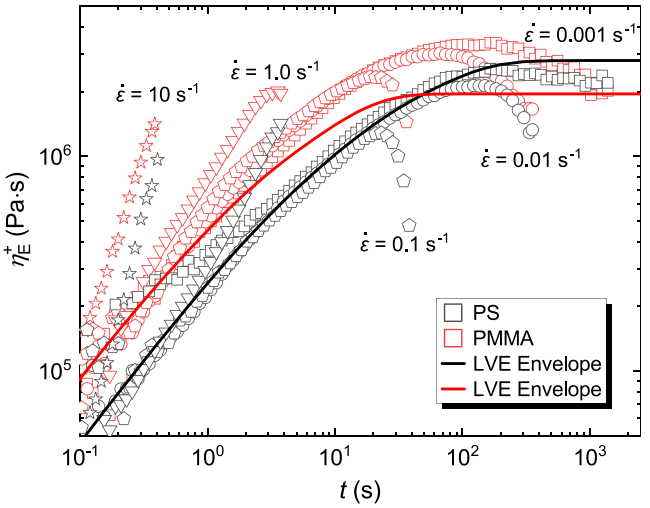

Figure 2. Extensional viscosity of PS and PMMA melts as a function of time at 155 °C at five chosen Hencky strain rates: 0.001, 0.01, 0.1, 1, and 10 s^{-1}. The solid lines represent the LVE envelope determined by the Maxwell model.

Hencky strain rates. The studied polymers exhibit comparable viscoelastic properties in SAOS; therefore, it is expected that extension properties will also be similar. As seen in Figure 2, PS at low strain rates (0.001 to 0.1 s^{-1}) follows the linear viscoelastic (LVE) envelope at the beginning of the measurement, e.g., at lower strain. However, toward higher measurement times, closer to the sample breakage, extensional viscosity decreases in comparison with the LVE values. This can be due to the necking of the samples, which can occur at these strain rates or indicate a strain-softening behavior related to chain stiffness.[30] Conversely, at high strain rates (1 and 10 s^{-1}), strain-hardening is observed. This can be explained by the fact that elastic forces overcome the viscous ones, as revealed by the Weissenberg number,[51] $Wi = \dot{\varepsilon}\lambda$, higher than 1. Here, λ is the terminal relaxation time of PS at 155 °C (taken from the crossing of G' and G'' in SAOS; see Figure S3) ≈7 s. The measured extensional viscosity increases more rapidly than the LVE and continues to a plateau value outside of the LVE regime,[52,53] which was not fully reached before breakage in the

https://doi.org/10.1021/acs.macromol.3c00288
Macromolecules 2023, 56, 6222−6231

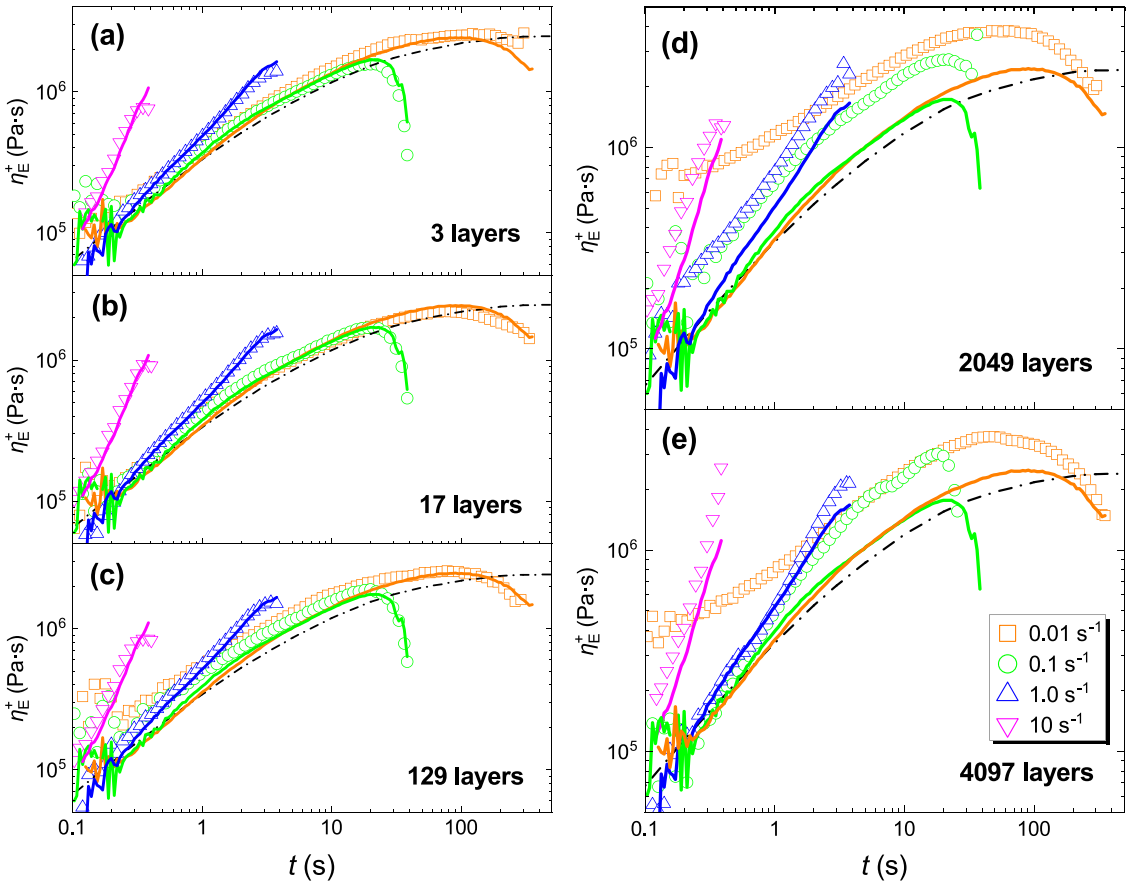

Figure 3. Extensional viscosity for four Hencky strain rates of films with various numbers of layers: (a) 3, (b) 17, (c) 129, (d) 2049, and (e) 4097 layers. The solid lines represent the additivity rule calculated from eq 4 with data of pure PS and PMMA for each strain rate, and the dashed lines represent the additivity rule of LVE data. The composition of the presented films is close to 60/40 PS/PMMA in all cases (see Table S2 for details).

present case. The data obtained for PS are in good agreement with the measurements performed by Bach et al.[54] and Huang et al.[24,26,53,55] on PS melts using a filament stretching rheometer (FSR). Though the experiments were performed at lower temperatures (120 or 130 °C), the PS response was analogous to our experiments. Strain-hardening was observed for the highest tested Hencky strain rates, while steady-state viscosity values were observed for lower strain rates. Here, the steady-state viscosity plateau was not observed, probably due to the restriction of one drum revolution in SER, while the FSR can reach higher strains.

Similarly to PS, PMMA exhibits strain-hardening at high strain rates. The relaxation time is about 2 s, and the strain rate at which *Wi* is higher than 1 is 0.5 s^{-1}. At lower strain rates, even though PMMA is closer to a regime of weak linear flow, the LVE envelope is only followed at the beginning of the measurements and a deviation toward higher viscosity values is noted.[27,56] In contrast, toward the sample breakage, necking and/or strain-softening due to chain stiffness[57,58] are observed, similarly to PS samples.[27,28]

Multilayer Films. The extensional viscosity of the 60/40 PS/PMMA multilayer films with various numbers of layers ($\eta^+_{E,M}$) is presented as a function of time in Figure 3. In order to understand the behavior of the multilayer films, a theoretical value of their viscosity was calculated at each Hencky strain rate. In a first simple approach[33,59] and following the theoretical framework initially developed by Macosko and co-workers,[34] we assume that the stress within the multilayer film ($\sigma^+_{E,M}$), which is proportional to the extensional viscosity and the overall extension rate, follows a simple additivity rule, and hence is a sum of stresses gathered within each component, PS layers and PMMA layers, following eq 4

$$\sigma^+_{E,M}(t) = \eta^+_E(t)\dot{\varepsilon} = \varphi_{PS}\sigma^+_{E,PS}(t) + \varphi_{PMMA}\sigma^+_{E,PMMA}(t) \quad (4)$$

where φ_{PS} and φ_{PMMA} are the volume fractions of PS and PMMA, respectively. The melt volume fractions of both PS and PMMA were corrected with a melt volume ratio including the variation in density values of the materials at room temperature and experimental temperature (see eq S5). The calculations of the additivity rule were done by using the extensional viscosity data of neat polymer melts presented in Figure 2.

The prediction of the LVE envelope for multilayer films was also calculated with a similar approach, using the respective LVE envelopes of PS and PMMA obtained through the Maxwell model.

As presented in Figure 3 for the 60/40 PS/PMMA composition, this basic additivity rule describes well the experimental data for all strain rates in the case of samples with 3, 17, and 129 layers. All three samples display behavior similar to that of PS and PMMA, as expected. At low strain rates, a strain-softening behavior is observed toward the end of the measurement, closer to breakage. At high strain rates, a strain-hardening is observed, similar to the neat polymer melts, hence

https://doi.org/10.1021/acs.macromol.3c00288
Macromolecules 2023, 56, 6222−6231

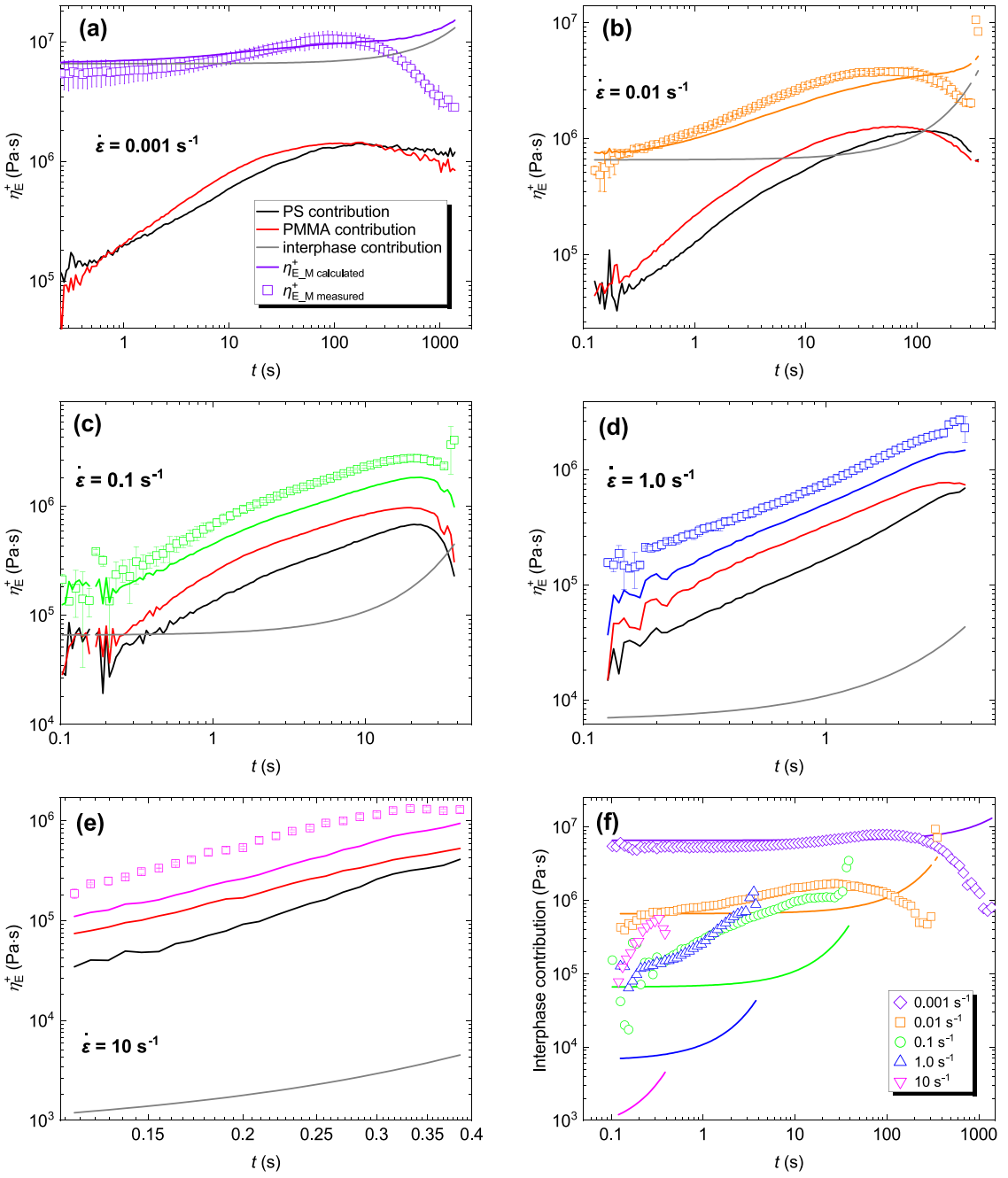

Figure 4. Comparison between experimental data (colored open symbols) and the additivity rule with the interphase for the extensional viscosity of the film with the 60/40 PS/PMMA composition and 2049 layers. The solid black, red, and gray lines represent each contribution from the model (PS, PMMA, and interphase, respectively), while the colored line is the sum of these three contributions. Each figure presents experiments done at different strain rates: (a) 0.001, (b) 0.01, (c) 0.1, (d) 1, and (e) 10 s^{-1}. (f) Comparison between the theoretical (solid lines) and measured values of the interphase contribution (colored open symbols).

well-captured by the additivity rule. On the other hand, samples with 2049 and 4097 layers display much different behavior. Starting with the lowest tested strain rate, 0.01 s^{-1}, a large increase in the values of $\eta^+_{E,M}$ compared to the prediction from eq 4 is observed from the very beginning of the measurement.[25,60] Though less pronounced at higher strain rates, the same observations can be made at all strain rates. Note that similar behavior is observed for the 30/70 PS/PMMA composition (see Figure S4). In the films with 2049 and 4097 layers, the number of interfaces is, as stated previously, extremely high. Though PS and PMMA display poor compatibility, their chains will still slightly interpenetrate at the interface, creating what we will call in the following an interphase of typical thickness:[61]

$$a_{int} \approx \frac{2b}{\sqrt{6\chi}} \tag{5}$$

where χ is the Flory–Huggins interaction parameter and b is the effective length per monomer unit[61] for which PS and PMMA have similar values,[62] b_{PS} = 6.8 Å[63] and b_{PMMA} = 7.4 Å.[64] To obtain χ at 155 °C, we use the well-known relation proposed by Russell et al.,[65] leading to $\chi \approx 0.037$, which gives

https://doi.org/10.1021/acs.macromol.3c00288
Macromolecules 2023, 56, 6222−6231

an interphase thickness close to 3 nm. This low value, smaller than the entanglement length (~7 nm),[66,67] is, as discussed in the introduction, notably responsible for the weak interfacial adhesion between these two polymers in the glassy state.[68]

Still, in films where the layer thicknesses are on the order of 100 nm (see Table S2), the interphase volume fraction becomes non-negligible, especially since it will increase during the rheological test, which slims down the film. To take into account this possible effect of the interphase in the extensional viscosity of multilayer films, Macosko and co-workers[34,35] proposed a refined version of the additivity rule incorporating the interfacial contribution

$$\sigma^{+}_{E,M}(t) = \varphi_{PS}\sigma^{+}_{E,PS}(t) + \varphi_{PMMA}\sigma^{+}_{E,PMMA}(t) + \varphi_{int}\sigma^{+}_{E,int}(t) \quad (6)$$

where φ_{int} and $\sigma^{+}_{E,int}$ are the volume fraction and the stress of the interphase, respectively (note that taking into account the interphase, the volume fractions of PS and PMMA layers in eqs 4 and 6 are then slightly different from each other for a given film).

φ_{int} is here simply defined as the total thickness of the interphase (the interphase thickness multiplied by the number of interfaces) divided by the total thickness of the film

$$\varphi_{int} = \frac{H_{int}}{H_M} = \frac{a_{int}(n-1)}{H_M} \quad (7)$$

We have to consider that during the measurement, the dimensions of the sample vary with time and strain (see the Supporting Information, eqs S2−S4). Especially, H_M is predicted to decrease exponentially, and the layers' continuity is assumed during all of the experiments. That was verified experimentally, as described in Figures S5 and S6. Therefore, if we make the hypothesis that the interphase typical thickness does not evolve significantly during the test (which will be discussed further later), then the fraction of the interphase will gradually increase over the experiment time. Assuming the chains are not oriented at the interfaces (i.e., for low *Wi*), the interfacial stress ($\sigma^{+}_{E,int}$) at equilibrium can be related to interfacial tension (Γ) and interphase thickness through the relation[35]

$$\sigma^{+}_{E,int}(t) = \frac{\Gamma}{a_{int}} \quad (8)$$

Substituting the stress with viscosity, the following equation describing the extensional viscosity of the multilayer film can be obtained[35]

$$\eta^{+}_{E,M}(t) = \varphi_{PS}\eta^{+}_{E,PS}(t) + \varphi_{PMMA}\eta^{+}_{E,PMMA}(t) + \frac{\Gamma(n-1)}{\dot{\varepsilon}H_0 \exp\left(\frac{-\dot{\varepsilon}t}{2}\right)} \quad (9)$$

Interfacial tension can be obtained, as the interfacial thickness, from the theoretical work of Helfand[61,69]

$$\Gamma = \frac{kT}{b^2}\left(\frac{\chi}{6}\right)^{1/2} \quad (10)$$

where k is the Boltzmann constant. The obtained value at 155 °C is 0.92 mN/m, similar to the one that can be extrapolated from Wu's experimental work (1.45 mN/m).[62,70]

The model predictions with no adjustable parameters are then compared to the experimental measurements for a chosen film (60/40 PS/PMMA composition, 2049 layers) in Figure 4 (see Figure S7 for the other composition). First, we should note that this approach is different from the one proposed by Jordan,[35] in which the interphase thickness was considered constant but Γ was a fitting parameter. Second, we can verify that for films with a small number of layers, the interfacial contribution is negligible and only improves marginally the fitting of the data (see Figure S8). It is seen in Figure 4 that at low strain rates, 0.001 and 0.01 s^{-1}, the experimental values are in good agreement with the model except close to the breaking point (see Figure 4a,b) since the model does not predict strain-softening but on the contrary, a slight strain-hardening due to an increase of the interfacial contribution related to the thinning of the sample over time. If we use Jordan's approach, the best fit is obtained for an interfacial tension of 0.75 mN/m, in good agreement with the calculated value (0.92 mN/m). With an increasing strain rate, an increasing deviation from the experimental value is observed. The model predicts that the interphase contribution at short times varies inversely proportionally to the strain rate, which leads to significant underestimates of the extensional viscosity of the multilayer films at strain rates above 0.1 s^{-1}. If we again use Jordan's approach in this case, best fits are obtained for values of interfacial tension that increase drastically with the strain rate, up to values much higher than the surface tension of PS and PMMA (see Figure S9). To gain more insight into the origin of this "dynamic" interfacial tension that can be extracted from Jordan's model and is much different from the equilibrium one (see eq 5), we then try to estimate what would be the necessary contribution to match the experimental data by subtracting the response of PS and PMMA from the multilayer one. Figure 4f presents a comparison of the interphase contribution calculated from eq 8 and extracted from our experimental results. As anticipated from the previous discussion, the contributions are similar at low strain rates and deviate strongly from each other at high strain rates. While under the hypotheses of the model, the interphase contribution is inversely proportional to the strain rate, the experimental contribution decreases less sharply and reaches similar viscosity values on the order from 10^5 to 10^6 Pa·s for strain rates higher than 0.1 s^{-1}. Similar conclusions can be drawn from the results presented in Figure S7 concerning the 30/70 PS/PMMA composition.

Interphase Properties. Let us now study the interfacial stress extracted from the experimental data presented in Figure 4 using eqs 6 and 9. The results for the same films as previously are presented as a function of strain, for each strain rate, in Figure 5 (interfacial stress for the film with 4097 layers and the other composition is presented in Figure S10). At thermodynamic equilibrium, the interfacial stress shall be constant, no matter what the strain and strain rate applied, and follow eq 8 with set values obtained from eqs 5 and 10. Note that by combining these three equations, this interfacial stress can be expressed as a function of the Flory interaction parameter and effective monomer length only

$$\sigma^{+}_{E,int,0}(t) = \frac{kT\chi}{2b^3} \approx 300\ \text{kPa} \quad (11)$$

which can be understood as the energy density of the monomers in the interphase.

From Figure 5, it is seen that this thermodynamic description of the interfacial stress describes the experimental data at low strains and strain rates. However, there is an

https://doi.org/10.1021/acs.macromol.3c00288
Macromolecules 2023, 56, 6222−6231

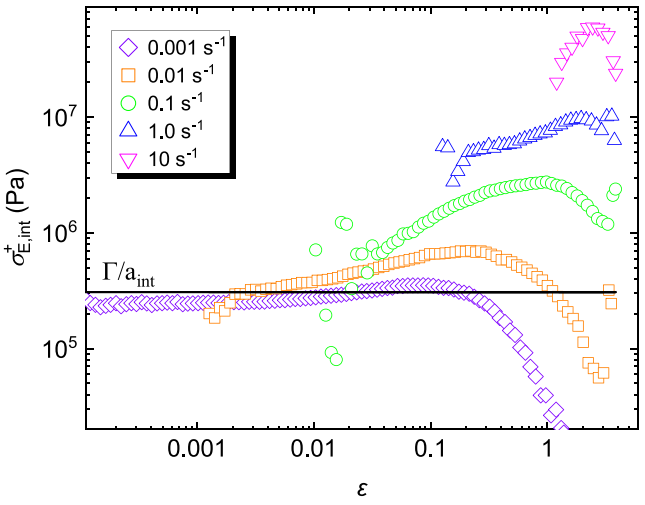

Figure 5. Measured interfacial stress as a function of strain for the same sample as in Figure 4.

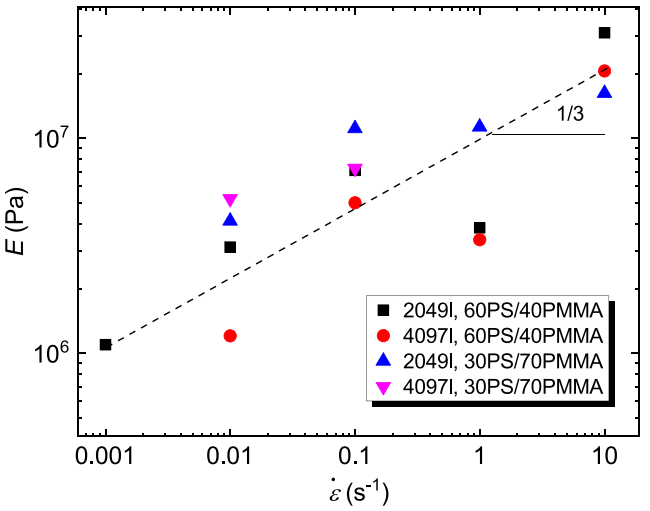

Figure 6. Interphase modulus as a function of the strain rate for films with 2049 and 4097 layers and 60/40 PS/PMMA and 30/70 PS/PMMA compositions.

increase in the interfacial stress as strain increases above a critical value (ε_c) close to 0.01, which becomes more pronounced at higher strain rates. This increase in stress may be due to the fact that the extensional flow modifies the interphase from its equilibrium conformation as the chains become oriented at high strains or at strain rates such as $Wi > 1$. In the bulk, the elasticity of polymer melts and solutions in shear flow manifests itself through the existence of two nonzero normal stress differences. It is thus tempting to say that accordingly, when subjected to strong elongations, the interphase response becomes nonisotropic; the tensile stress is two-dimensional (2D), analogous to this difference in normal stress, i.e., anisotropy of the surface tension in the film. This anisotropy of the surface tension with respect to the direction is the signature of the 2D elasticity of the interphase.[71] A similar phenomenon occurs in soap films, where the Gibbs−Marangoni surface elasticity is due to the dilution of the surfactant at the interface and is responsible for their stability.[72]

If we consider the region above the critical strain, then there is first a linear increase of the interphase contribution with strain, followed by a plateau and then a decrease before failure. Let us focus on the linear increase region (see Figure S11), in which we can write the interfacial stress as

$$\sigma^{+}_{E,int}(\varepsilon) = \sigma^{+}_{E,int,0} + E_{\dot{\varepsilon}}(\varepsilon - \varepsilon_c) \quad (12)$$

where the slope of the linear interfacial stress−strain region can then be termed an "interphase modulus" ($E_{\dot{\varepsilon}}$) by analogy with the Gibbs−Marangoni surface elasticity. Values from about 1 to ∼10 MPa, which are typical of a rubbery plateau modulus, are obtained for $E_{\dot{\varepsilon}}$ as the strain rate increases from 0.001 to 10 s^{-1}. Since this anisotropy is a dynamic effect, we observe a modulus that depends on the strain rate. Plotting this dependence of the modulus in Figure 6, we can see that similar values of the modulus are obtained at each strain rate for all samples and compositions, with a power-law dependence with the strain rate having an exponent of about 1/3.

As stated previously, this interphase modulus shall be related to conformational changes[73,74] close to the interface appearing at large strains and strain rates, but the precise description or modeling of the molecular dependency with respect to the strain rate is out of the scope of this paper. Still, the analogy with Gibbs elasticity and the existence of an interfacial modulus has also been discussed in the case of sheared compatibilized blends.[75,76] We can also note that the increase in modulus with the strain rate is widely documented for rubbers in the bulk and is a signature of the time−temperature superposition principle.[77] Additionally, changes in viscoelastic properties of elastomers due to confinement[78], as well as the effect of the strain rate on the modulus of free-standing glassy ultrathin polymer films, have been evidenced recently.[79]

We can conclude by injecting the empirical relation of eq 12 into eq 9. The values of E and ε_c previously obtained result in a much higher interphase contribution than predicted,[35] which captures much better the evolution of the extensional viscosity of the multilayer film with time up to necking, at all strain rates (and especially at larger ones), as shown in Figure S12.

CONCLUSIONS

A systematic study of the extensional properties of multilayer films of an immiscible polymer pair (PS/PMMA) has been conducted to probe the interphase rheological properties. A simple additivity rule based on the summation of forces within PS and PMMA captures well the response from multilayer films with up to 129 layers. As the number of layers increases, the volume fraction of the interphase becomes non-negligible. A refined model proposed by Jordan et al.,[35] which includes the interfacial contribution in the additivity rule, captures well the behavior of our systems with more than 2000 layers and at low strain rates. At high strain rates, however, the model underestimates the contribution of the interphase. Looking at the interfacial stress, a deviation from the thermodynamic equilibrium value related to interfacial tension and interphase thickness is observed at strains above a critical value of about 1%. A linear increase with strain is observed, with a slope increasing with increasing strain rate, leading to the measurement of an "interphase modulus", with values ranging from about 1 to 10 MPa. These values are those of a typical rubbery plateau modulus, even though such noncompatibilized interphases are unentangled, suggesting a different behavior from the bulk and reminiscent of interfacial phenomena such as Gibbs−Marangoni elasticity. With this study, it is shown that extensional viscosity measurements can be used as a probe

https://doi.org/10.1021/acs.macromol.3c00288
Macromolecules 2023, 56, 6222−6231

for determining the intrinsic "2D" rheological properties of interphases (i.e., interfacial rheology), even for non-compatibilized systems. Having evidenced a surface elasticity occurring at high strain rates, it could be relevant to study its impact on the stability of nanolayers in elongational flows during processing such as nanolayer coextrusion.

■ ASSOCIATED CONTENT

Supporting Information

The Supporting Information is available free of charge at https://pubs.acs.org/doi/10.1021/acs.macromol.3c00288.

Characteristics and viscoelastic properties of PS and PMMA used in the study; characteristics of the PS/PMMA multilayer films; Maxwell model fits and data of SAOS and the thermodependency parameter of PS and PMMA; extensional viscosity calculations and data for the 30/70 PS/PMMA composition; experimental validation of the exponential thinning; comparison between experimental data and additivity rule with interfacial contribution for the 30/70 PS/PMMA film with 2049 layers; comparison between models without and with interphase contribution for a 60/40 PS/PMMA film with 17 layers; measured interphase stress as a function of strain for films with 4097 layers; composition 60/40 PS/PMMA and 2049 and 4097 layers; 30/70 PS/PMMA composition; linear region of measured interphase stress as a function of strain; and comparison of the experimental data with the model taking into account the interphase contribution and the interphase elasticity in the sample with 2049 layers and 60/40 PS/PMMA composition (PDF)

■ AUTHOR INFORMATION

Corresponding Authors

Jorge Peixinho − *Laboratoire PIMM, CNRS, Arts et Métiers Institute of Technology, Cnam, HESAM Universite, 75013 Paris, France*; Email: jorge.peixinho@cnrs.fr

Guillaume Miquelard-Garnier − *Laboratoire PIMM, CNRS, Arts et Métiers Institute of Technology, Cnam, HESAM Universite, 75013 Paris, France*; orcid.org/0000-0002-0251-8941; Email: guillaume.miquelardgarnier@lecnam.net

Authors

Anna Dmochowska − *Laboratoire PIMM, CNRS, Arts et Métiers Institute of Technology, Cnam, HESAM Universite, 75013 Paris, France*

Cyrille Sollogoub − *Laboratoire PIMM, CNRS, Arts et Métiers Institute of Technology, Cnam, HESAM Universite, 75013 Paris, France*; orcid.org/0000-0003-2204-3696

Complete contact information is available at: https://pubs.acs.org/10.1021/acs.macromol.3c00288

Notes

The authors declare no competing financial interest.

■ ACKNOWLEDGMENTS

The authors thank Alexis Chennevière for providing relevant references. They deeply acknowledge Frédéric Restagno for helpful suggestions on data analysis and interpretation. We also thank him and Ilias Iliopoulos for critical reading of the manuscript. The Ecole Doctorale SMI (ED 432) is acknowledged for granting A.D. the fellowship for her Ph.D. work.

■ REFERENCES

(1) Utracki, L. A. *Commercial Polymer Blends*; Springer, 1998.

(2) Formela, K.; Zedler, L.; Hejna, A.; Tercjak, A. Reactive extrusion of bio-based polymer blends and composites - Current trends and future developments. *eXPRESS Polym. Lett.* **2018**, *12*, 24−57.

(3) Bousmina, M.; Qiu, H.; Grmela, M.; Klemberg-Sapieha, J. E. Diffusion at polymer/polymer interfaces probed by rheological tools. *Macromolecules* **1998**, *31*, 8273−8280.

(4) Xing, P.; Bousmina, M.; Rodrigue, D.; Kamal, M. R. Critical Experimental Comparison between Five Techniques for the Determination of Interfacial Tension in Polymer Blends: Model System of Polystyrene/Polyamide-6. *Macromolecules* **2000**, *33*, 8020−8034.

(5) Kwon, T.; Kim, T.; Ali, F. b.; Kang, D. J.; Yoo, M.; Bang, J.; Lee, W.; Kim, B. J. Size-Controlled Polymer-Coated Nanoparticles as Efficient Compatibilizers for Polymer Blends. *Macromolecules* **2011**, *44*, 9852−9862.

(6) de Luna, M. S.; Filippone, G. Effects of nanoparticles on the morphology of immiscible polymer blends − Challenges and opportunities. *Eur. Polym. J.* **2016**, *79*, 198−218.

(7) Qiao, H.; Zheng, B.; Zhong, G.; Li, Z.; Cardinaels, R.; Moldenaers, P.; Lamnawar, K.; Maazouz, A.; Liu, C.; Zhang, H. Understanding the Rheology of Polymer-Polymer Interfaces Covered with Janus Nanoparticles: Polymer Blends versus Particle Sandwiched Multilayers. *Macromolecules* **2023**, *56*, 647−663.

(8) Zhang, G.; Yang, H.; He, L.; Hu, L.; Lan, S.; Li, F.; Chen, H.; Guo, T. Importance of domain purity in semi-conducting polymer/insulating polymer blends transistors. *J. Polym. Sci., Part B: Polym. Phys.* **2016**, *54*, 1760−1766.

(9) Fredrickson, G. H.; Xie, S.; Edmund, J.; Le, M. L.; Sun, D.; Grzetic, D. J.; Vigil, D. L.; Delaney, K. T.; Chabinyc, M. L.; Segalman, R. A. Ionic Compatibilization of Polymers. *ACS Polym. Au* **2022**, *2*, 299−312.

(10) Benmouna, M.; Vilgis, T. A. Scattering from multicomponent polymer mixtures: weakly charged polymers. *Macromolecules* **1991**, *24*, 3866−3872.

(11) Creton, C.; Kramer, E. J.; Hadziioannou, G. Critical molecular weight for block copolymer reinforcement of interfaces in a two-phase polymer blend. *Macromolecules* **1991**, *24*, 1846−1853.

(12) Creton, C.; Kramer, E. J.; Hui, C. Y.; Brown, H. R. Failure mechanisms of polymer interfaces reinforced with block copolymers. *Macromolecules* **1992**, *25*, 3075−3088.

(13) Beuguel, Q.; Guinault, A.; Leger, L.; Restagno, F.; Sollogoub, C.; Miquelard-Garnier, G. Nanorheology with a conventional rheometer: Probing the interfacial properties in compatibilized multinanolayer polymer films. *ACS Macro Lett.* **2019**, *8*, 1309−1315.

(14) Beuguel, Q.; Guinault, A.; Chinesta, F.; Sollogoub, C.; Miquelard-Garnier, G. Modeling of the rheological properties of multinanolayer films in the presence of compatibilized interphase. *J. Rheol.* **2020**, *64*, 981−989.

(15) Li, Z.; Olah, A.; Baer, E. Micro-and nano-layered processing of new polymeric systems. *Prog. Polym. Sci.* **2020**, *102*, No. 101210.

(16) Baer, E.; Zhu, L. 50th anniversary perspective: dielectric phenomena in polymers and multilayered dielectric films. *Macromolecules* **2017**, *50*, 2239−2256.

(17) Brown, H. R. Relation between the Width of an Interface between Two Polymers and Its Toughness. *Macromolecules* **2001**, *34*, 3720−3724.

(18) Palierne, J. F. Linear rheology of viscoelastic emulsions with interfacial tension. *Rheol. Acta* **1990**, *29*, 204−214.

(19) Graebling, D.; Muller, R. M.; Palierne, J.-F. Linear viscoelasticity of incompatible polymer blends in the melt in relation with interfacial properties. *J. Phys. IV* **1993**, *03*, 1525−1534.

(20) Xing, P.; Bousmina, M.; Rodrigue, D.; Kamal, M. R. Critical experimental comparison between five techniques for the determi-

nation of interfacial tension in polymer blends: Model system of polystyrene/polamide-6. *Macromolecules* **2000**, *33*, 8020−8034.
(21) El Omari, Y.; Yousfi, M.; Duchet-Rumeau, J.; Maazouz, A. Recent Advances in the Interfacial Shear and Dilational Rheology of Polymer Systems: From Fundamentals to Applications. *Polymers* **2022**, *14*, No. 2844, DOI: 10.3390/polym14142844.
(22) Thomas, S.; Shanks, R.; Chandran, S. *Design and Applications of Nanostructured Polymer Blends and Nanocomposite Systems*; William Andrew, 2015.
(23) Doi, M.; Edwards, S. F. *The Theory of Polymer Dynamics*; Oxford University Press, 1988; Vol. *73*.
(24) Huang, Q. When Polymer Chains Are Highly Aligned: A Perspective on Extensional Rheology. *Macromolecules* **2022**, *55*, 715−727.
(25) Andrade, R. J.; Harris, P.; Maia, J. High strain extensional rheometry of polymer melts: Revisiting and improving the Meissner design. *J. Rheol.* **2014**, *58*, 869−890.
(26) Huang, Q.; Hengeller, L.; Alvarez, N. J.; Hassager, O. Bridging the gap between polymer melts and solutions in extensional rheology. *Macromolecules* **2015**, *48*, 4158−4163.
(27) Stamboulides, C.; Hatzikiriakos, S. G. Rheology and processing of molten poly (methyl methacrylate) resins. *Int. Polym. Process.* **2006**, *21*, 155−163.
(28) Morelly, S. L.; Palmese, L.; Watanabe, H.; Alvarez, N. J. Effect of finite extensibility on nonlinear extensional rheology of polymer melts. *Macromolecules* **2019**, *52*, 915−922.
(29) Zhang, H.; Lamnawar, K.; Maazouz, A. Rheological modeling of the diffusion process and the interphase of symmetrical bilayers based on PVDF and PMMA with varying molecular weights. *Rheol. Acta* **2012**, *51*, 691−711.
(30) Zhang, H.; Lamnawar, K.; Maazouz, A.; Maia, J. M. A nonlinear shear and elongation rheological study of interfacial failure in compatible bilayer systems. *J. Rheol.* **2016**, *60*, 1−23.
(31) Lu, B.; Lamnawar, K.; Maazouz, A.; Sudre, G. Critical Role of Interfacial Diffusion and Diffuse Interphases Formed in Multi-Micro-/Nanolayered Polymer Films Based on Poly(vinylidene fluoride) and Poly(methyl methacrylate). *ACS Appl. Mater. Interfaces.* **2018**, *10*, 29019−29037.
(32) Zhao, W.; Zhang, M.; Zhang, H.; Shen, J.; Lu, B.; Dong, B.; Liu, C.; Maazouz, A.; Lamnawar, K. Roles of Interlayer Diffusion and Confinements in Manipulating Microstructural Evolutions in Multilayer Assembled Polyvinylidene Fluoride/Poly(methyl methacrylate) Films for Tunable Dielectric and Piezoelectric Performances. *ACS Appl. Polym. Mater.* **2021**, *3*, 3843−3854.
(33) Lu, B.; Bondon, A.; Touil, I.; Zhang, H.; Alcouffe, P.; Pruvost, S.; Liu, C.; Maazouz, A.; Lamnawar, K. Role of the macromolecular architecture of copolymers at layer-layer interfaces of multilayered polymer films: A combined morphological and rheological investigation. *Ind. Eng. Chem. Res.* **2020**, *59*, 22144−22154.
(34) Levitt, L.; Macosko, C. W.; Schweizer, T.; Meissner, J. Extensional rheometry of polymer multilayers: A sensitive probe of interfaces. *J. Rheol.* **1997**, *41*, 671−685.
(35) Jordan, A. M.; Lee, B.; Kim, K.; Ludtke, E.; Lhost, O.; Jaffer, S. A.; Bates, F. S.; Macosko, C. W. Rheology of polymer multilayers: Slip in shear, hardening in extension. *J. Rheol.* **2019**, *63*, 751−761.
(36) Bironeau, A.; Salez, T.; Miquelard-Garnier, G.; Sollogoub, C. Existence of a Critical Layer Thickness in PS/PMMA Nanolayered Films. *Macromolecules* **2017**, *50*, 4064−4073.
(37) Zhu, Y.; Bironeau, A.; Restagno, F.; Sollogoub, C.; Miquelard-Garnier, G. Kinetics of thin polymer film rupture: Model experiments for a better understanding of layer breakups in the multilayer coextrusion process. *Polymer* **2016**, *90*, 156−164.
(38) Plazek, D. J. Temperature dependence of the viscoelastic behavior of polystyrene. *J. Phys. Chem. A* **1965**, *69*, 3480−3487.
(39) Bird, R. B.; Carreau, P. J. A nonlinear viscoelastic model for polymer solutions and melts-I. *Chem. Eng. Sci.* **1968**, *23*, 427−434.
(40) Dmochowska, A.; Peixinho, J.; Sollogoub, C.; Miquelard-Garnier, G. Dewetting Dynamics of Sheared Thin Polymer Films: An Experimental Study. *ACS Macro Lett.* **2022**, *11*, 422−427.
(41) Montana, J.-S.; Roland, S.; Richaud, E.; Miquelard-Garnier, G. Nanostructuration effect on the mechanical properties of PMMA toughened by a triblock acrylate copolymer using multilayer coextrusion. *Polymer* **2018**, *149*, 124−133.
(42) Bironeau, A.; Dirrenberger, J.; Sollogoub, C.; Miquelard-Garnier, G.; Roland, S. Evaluation of morphological representative sample sizes for nanolayered polymer blends. *J. Microsc.* **2016**, *264*, 48−58.
(43) Sentmanat, M. L. Miniature universal testing platform: from extensional melt rheology to solid-state deformation behavior. *Rheol. Acta* **2004**, *43*, 657−669.
(44) Sentmanat, M.; Wang, B. N.; McKinley, G. H. Measuring the transient extensional rheology of polyethylene melts using the SER universal testing platform. *J. Rheol.* **2005**, *49*, 585−606.
(45) Costanzo, S.; Pasquino, R.; Läuger, J.; Grizzuti, N. Milligram Size Rheology of Molten Polymers. *Fluids* **2019**, *4*, No. 28, DOI: 10.3390/fluids4010028.
(46) Andrade, R. J.; Harris, P.; Maia, J. M. High strain extensional rheometry of polymer melts: Revisiting and improving the Meissner design. *J. Rheol.* **2014**, *58*, 869−890.
(47) Hirschberg, V.; Lyu, S.; Schussmann, M. G. Complex polymer topologies in blends: Shear and elongational rheology of linear/pom-pom polystyrene blends. *J. Rheol.* **2023**, *67*, 403−415.
(48) Bourg, V.; Valette, R.; Le Moigne, N.; Ienny, P.; Guillard, V.; Bergeret, A. Shear and Extensional Rheology of Linear and Branched Polybutylene Succinate Blends. *Polymers* **2021**, *13*, No. 652, DOI: 10.3390/polym13040652.
(49) Barnes, H. A.; Hutton, J. F.; Walters, K. *An Introduction to Rheology*; Elsevier, 1989.
(50) Dealy, J. M.; Read, D. J.; Larson, R. G. *Structure and Rheology of Molten Polymers: from Structure to Flow Behavior and Back Again*, 2nd ed.; Hanser Publisher, 2018.
(51) Thompson, R. L.; Oishi, C. M. Reynolds and Weissenberg numbers in viscoelastic flows. *J. Non-Newtonian Fluid Mech.* **2021**, *292*, No. 104550.
(52) Matsumiya, Y.; Watanabe, H.; Masubuchi, Y.; Huang, Q.; Hassager, O. Nonlinear Elongational Rheology of Unentangled Polystyrene and Poly(p-tert-butylstyrene) Melts. *Macromolecules* **2018**, *51*, 9710−9729.
(53) Huang, Q.; Rasmussen, H. K. Extensional flow dynamics of polystyrene melt. *J. Rheol.* **2019**, *63*, 829−835.
(54) Bach, A.; Almdal, K.; Rasmussen, H. K.; Hassager, O. Elongational Viscosity of Narrow Molar Mass Distribution Polystyrene. *Macromolecules* **2003**, *36*, 5174−5179.
(55) Huang, Q.; Mednova, O.; Rasmussen, H. K.; Alvarez, N. J.; Skov, A. L.; Almdal, K.; Hassager, O. Concentrated Polymer Solutions are Different from Melts: Role of Entanglement Molecular Weight. *Macromolecules* **2013**, *46*, 5026−5035.
(56) Rasmussen, H. K.; Wingstrand, S. L.; Hassager, O. On the universality in the extensional rheology of monodisperse polymer melts and oligomer dilutions thereof. *Rheol. Acta* **2019**, *58*, 333−340.
(57) Iisaka, K.; Yama, K. S. Mechanical α-dispersion and interaction in filled polystyrene and polymethylmethacrylate. *J. Appl. Polym. Sci.* **1978**, *22*, 3135−3143.
(58) Javadi, S.; Panahi-Sarmad, M.; Razzaghi-Kashani, M. Interfacial and dielectric behavior of polymer nano-composites: effects of chain stiffness and cohesive energy density. *Polymer* **2018**, *145*, 31−40.
(59) Lu, B.; Lamnawar, K.; Maazouz, A. Influence of in situ reactive interphase with graft copolymer on shear and extensional rheology in a model bilayered polymer system. *Polym. Test.* **2017**, *61*, 289−299.
(60) Nielsen, J. K.; Hassager, O.; Rasmussen, H. K.; McKinley, G. H. Observing the chain stretch transition in a highly entangled polyisoprene melt using transient extensional rheometry. *J. Rheol.* **2009**, *53*, 1327−1346.
(61) Helfand, E.; Tagami, Y. Theory of the Interface between Immiscible Polymers. II. *J. Chem. Phys.* **1972**, *56*, 3592−3601.
(62) Miquelard-Garnier, G.; Roland, S. Beware of the Flory parameter to characterize polymer-polymer interactions: A critical

reexamination of the experimental literature. *Eur. Polym. J.* **2016**, *84*, 111−124.
(63) Ballard, D. G. H.; Wignall, G. D.; Schelten, J. Measurement of molecular dimensions of polystyrene chains in the bulk polymer by low angle neutron diffraction. *Eur. Polym. J.* **1973**, *9*, 965−969.
(64) Kirste, V. R. G. Neue vorstellungen über statistische fadenknäuel. *Die Makromol. Chem.* **1967**, *101*, 91−103.
(65) Russell, T. P.; Hjelm, R. P.; Seeger, P. A. Temperature dependence of the interaction parameter of polystyrene and poly(methyl methacrylate). *Macromolecules* **1990**, *23*, 890−893.
(66) Fetters, L. J.; Lohse, D. J.; Richter, D.; Witten, T. A.; Zirkel, A. Connection between Polymer Molecular Weight, Density, Chain Dimensions, and Melt Viscoelastic Properties. *Macromolecules* **1994**, *27*, 4639−4647.
(67) Fetters, L. J.; Lohse, D. J.; Milner, S. T.; Graessley, W. W. Packing Length Influence in Linear Polymer Melts on the Entanglement, Critical, and Reptation Molecular Weights. *Macromolecules* **1999**, *32*, 6847−6851.
(68) Schnell, R.; Stamm, M.; Creton, C. Direct Correlation between Interfacial Width and Adhesion in Glassy Polymers. *Macromolecules* **1998**, *31*, 2284−2292.
(69) Helfand, E.; Tagami, Y. Theory of the interface between immiscible polymers. *J. Polym. Sci., Part B: Polym. Lett.* **1971**, *9*, 741−746.
(70) Wu, S. Surface and interfacial tensions of polymer melts. II. Poly(methyl methacrylate), poly(n-butyl methacrylate), and polystyrene. *J. Phys. Chem. A* **1970**, *74*, 632−638.
(71) *Interfacial Rheology*; Miller, R.; Liggieri, L., Eds.; CRC Press, Taylor & Francis Group: Boca Raton London New York, 2019.
(72) Gibbs, W. *The Scientific Papers*; Dover: New-York, 1961.
(73) Cunha, M. A. G.; Robbins, M. O. Effect of flow-induced molecular alignment on welding and strength of polymer interfaces. *Macromolecules* **2020**, *53*, 8417−8427.
(74) Zhang, T.; Wang, N.; Riggleman, R. A. Failure and Mechanical Properties of Glassy Diblock Copolymer Thin Films. *Macromolecules* **2022**, *55*, 10880−10890.
(75) Riemann, R.-E.; Cantow, H.-J.; Friedrich, C. Interpretation of a New Interface-Governed Relaxation Process in Compatibilized Polymer Blends. *Macromolecules* **1997**, *30*, 5476−5484.
(76) Jacobs, U.; Fahrländer, M.; Winterhalter, J.; Friedrich, C. Analysis of Palierne's emulsion model in the case of viscoelastic interfacial properties. *J. Rheol.* **1999**, *43*, 1495−1509.
(77) Roland, C. M. Mechanical Behavior of Rubber at High Strain Rates. *Rubber Chem. Technol.* **2006**, *79*, 429−459.
(78) Bai, P.; Ma, M.; Sui, L.; Guo, Y. Nanoconfinement Controls Mechanical Properties of Elastomeric Thin Films. *J. Phys. Chem. Lett.* **2021**, *12*, 8072−8079.
(79) Yiu, P. M.; Yuan, H.; Gu, Q.; Gao, P.; Tsui, O. K. C. Strain Rate and Thickness Dependences of Elastic Modulus of Free-Standing Polymer Nanometer Films. *ACS Macro Lett.* **2020**, *9*, 1521−1526.

https://doi.org/10.1021/acs.macromol.3c00288
Macromolecules 2023, 56, 6222−6231

Supporting Information for 'Extensional Viscosity of Immiscible Polymers Multinanolayer Films: Signature of the Interphase'

Anna Dmochowska, Jorge Peixinho,* Cyrille Sollogoub, and Guillaume Miquelard-Garnier*

Laboratoire PIMM, CNRS, Arts et Métiers Institute of Technology, Cnam, HESAM Universite, 75013 Paris, France

E-mail: jorge.peixinho@cnrs.fr; guillaume.miquelardgarnier@lecnam.net

Characteristics of polymers used in the study

Table S1: *Properties of the polymers used in the study. The molar masses (M_W) and dispersities ($Đ$) were measured by Zhu et al.[1]; glass transition temperatures (T_g) were obtained from differential scanning calorimetry measurements on a Q10 analyzer (TA Instruments); the density at room temperature ($\rho_{25°C}$) was taken from the supplier technical sheet, and the density at 225 °C ($\rho_{225°C}$) was measured by Bironeau et al.[2]*

Polymer	M_W (kg/mol)	$Đ$	T_g (°C)	$\rho_{25°C}$ (g/cm^3)	$\rho_{225°C}$ (g/cm^3)
PS	245	2.2	96	1.05	0.95
PMMA	139	2.1	94	1.18	1.07

Viscoelastic properties of the neat polymer melts

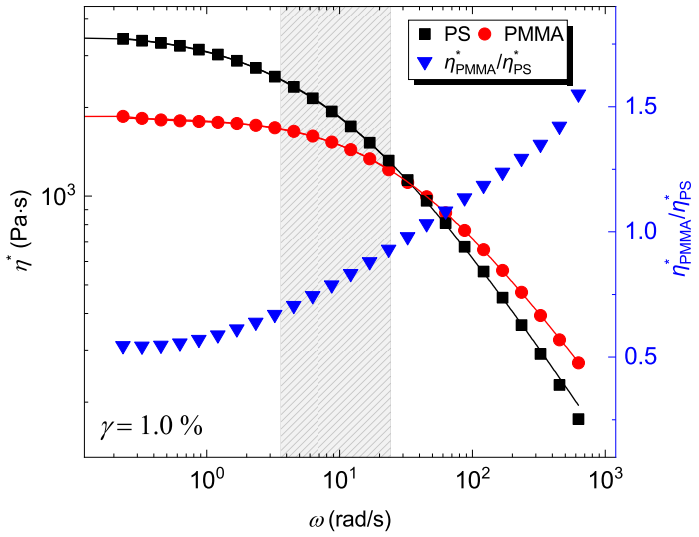

Figure S1: *Complex viscosity (η^*) of PS and PMMA as a function of angular frequency (ω) and their viscosity ratio at 225 °C and 1 % strain. The complex viscosity data were fitted with the Carreau-Yasuda model. The measurements were performed within the LVE region at shear strain 1 %. The gray area highlights the region corresponding to shear rate values found in our multilayer coextrusion setup when assuming the Cox-Merz rule.*[2]

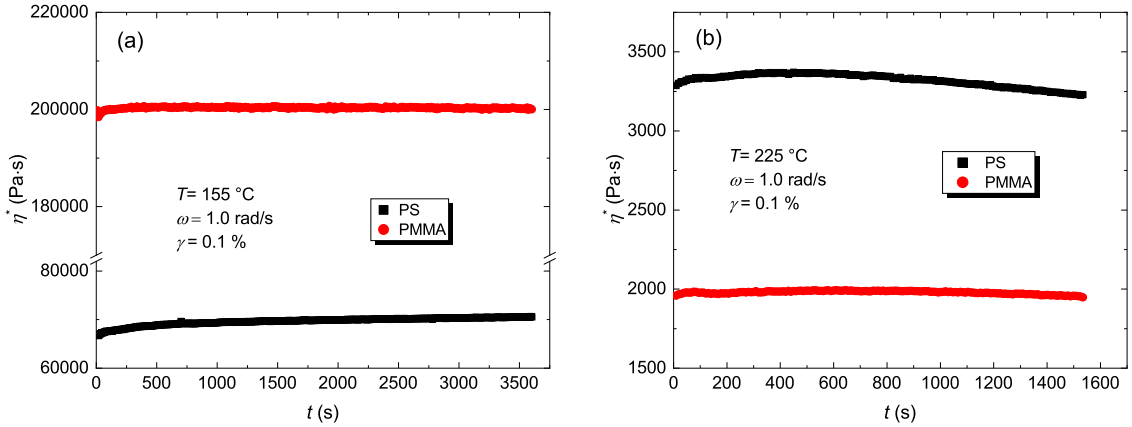

Figure S2: *Complex viscosity of PS and PMMA at 155 °C (a) and 225 °C (b) as a function of time. The measurements were performed within the LVE region at shear strain 0.1 % and with pulsation $\omega = 1$ rad/s. The maximum variation of viscosity values is 1.1 % for PS and 0.1 % for PMMA at 155 °C, and 4.5 % for PS and 0.5 % for PMMA at 225 °C, respectively.*

Characteristics of the fabricated PS/PMMA multilayer films

The theoretical thickness of the individual layer of each polymer can be calculated from the following equation:

$$h_{\mathrm{A}} = H_{\mathrm{M}} \times \frac{\phi_A}{n_A} \tag{S1}$$

where H_{M} is the total thickness of the multilayer film, ϕ_A is the volume fraction of polymer A in the film, and n_A the number of its layers. In the used coextrusion set-up, we start with the configuration A-B-A which in our case is PMMA-PS-PMMA. The number of layers n_A is calculated directly from the number of used LME with $n_A = 2^N + 1$. The equation is almost identical for polymer B (in our case PS) with $n_B = 2^N$.

Table S2: *Comparison of calculated and measured individual layer thicknesses.*

Fraction PS/PMMA (wt %)	Total no. of layers (n)	Film thickness (μm)	No. of measured layers	PS layer thickness		PMMA layer thickness	
				Calc. (nm)	Measured (nm)	Calc. (nm)	Measured (nm)
62/38	3	385 ± 39	3	186000	273700 ± 2300	83000	84500 ± 1400
60/40	17	587 ± 60	17	35200	453000 ± 5500	27800	27000 ± 2500
56/44	129	222 ± 20	30	1600	1800 ± 734	1400	1400 ± 570
57/43	2049	305 ± 16	240	131	159 ± 42	116	122 ± 29
56/44	2049	572 ± 45	220	298	287 ± 91	260	221 ± 78
53/47	4097	585 ± 87	425	115	124 ± 46	102	108 ± 34
53/47	4097	890 ± 72	438	232	198 ± 102	203	176 ± 77
29/71	3	607 ± 90	3	121000	192700 ± 12600	215000	237400 ± 7900
22/78	17	753 ± 39	17	19900	24000 ± 6600	70800	77200 ± 10300
19/81	129	799 ± 97	40	2800	2560 ± 700	9700	10440 ± 1700
25/75	2049	541 ± 37	240	106	132 ± 60	376	391 ± 91
26/74	4097	944 ± 47	425	90	111 ± 49	319	316 ± 104

Multimode Maxwell Model

Figure S3 reports the Time-Temperature superposition of SAOS data at reference temperature 155 °C of PS and PMMA together with the obtained fits of the 10-mode Maxwell model represented as lines. The relaxation moduli and time constants of the model are listed in Table S3. Note that the slope of G'' for PMMA at low reduced angular frequency is 1.7 rather than 2, as predicted by the Maxwell model, meaning we do not observe the terminal behavior[3]. The temperature behavior of both polymers is well captured by the WLF equation, in agreement with previous authors[4].

Table S3: *Linear Viscoelastic spectra for PS and PMMA at 155 °C.*

	PS		PMMA	
i	$\tau_i\,(s)$	$g_i\,(Pa)$	$\tau_i\,(s)$	$g_i\,(Pa)$
1	3.34×10^{0}	2.93×10^{4}	1.30×10^{0}	1.09×10^{5}
2	8.62×10^{-1}	4.14×10^{4}	1.94×10^{-1}	1.33×10^{5}
3	6.00×10^{-5}	1.74×10^{6}	2.73×10^{-3}	1.69×10^{5}
4	3.20×10^{-4}	4.00×10^{5}	3.90×10^{-5}	4.22×10^{6}
5	1.49×10^{-1}	5.25×10^{4}	1.05×10^{1}	4.54×10^{4}
6	1.35×10^{1}	1.93×10^{4}	3.80×10^{-5}	6.96×10^{5}
7	2.65×10^{-3}	1.88×10^{5}	2.74×10^{-3}	1.51×10^{5}
8	5.39×10^{-6}	2.30×10^{7}	2.60×10^{-2}	1.54×10^{5}
9	2.52×10^{-2}	5.37×10^{4}	4.50×10^{-4}	4.91×10^{5}
10	7.63×10^{1}	6.91×10^{3}	3.80×10^{-5}	2.68×10^{6}

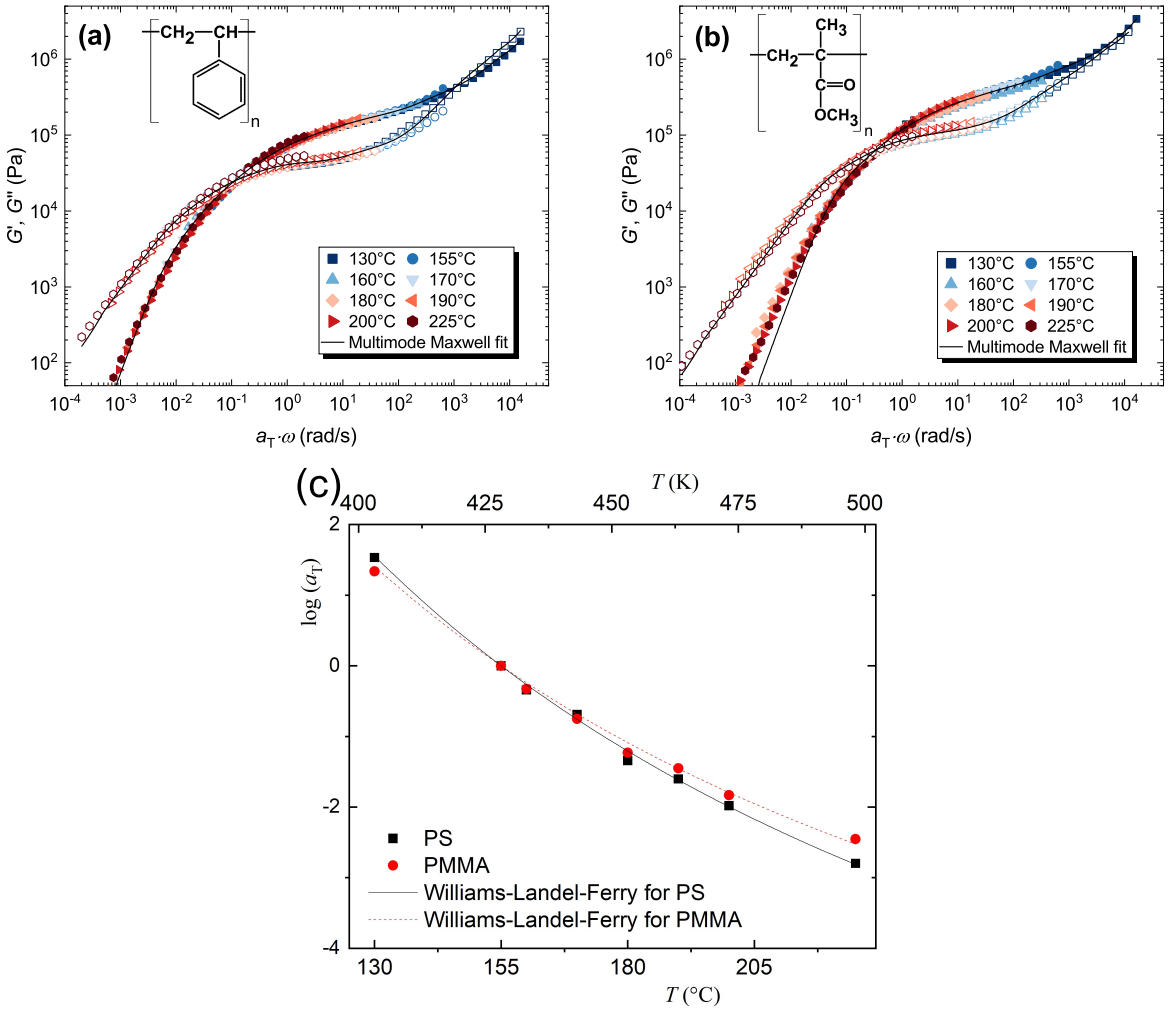

Figure S3: *Storage (G', open symbols) and loss (G'', closed symbols) moduli as a function of reduced angular frequency ($a_T\omega$) for PS (a) and PMMA (b). The superposition was done at $T_{ref} = 155$ °C. The lines represent the Maxwell fit described in the main body of the manuscript. (c) The shift factor, a_T, as a function of temperature. The lines represent the Williams-Landel-Ferry (WLF) equation: $\log a_T = -C_1 (T - T_{ref}) / (C_2 + T - T_{ref})$, where C_1 and C_2 are adjusted parameters.*

Extensional viscosity measurements

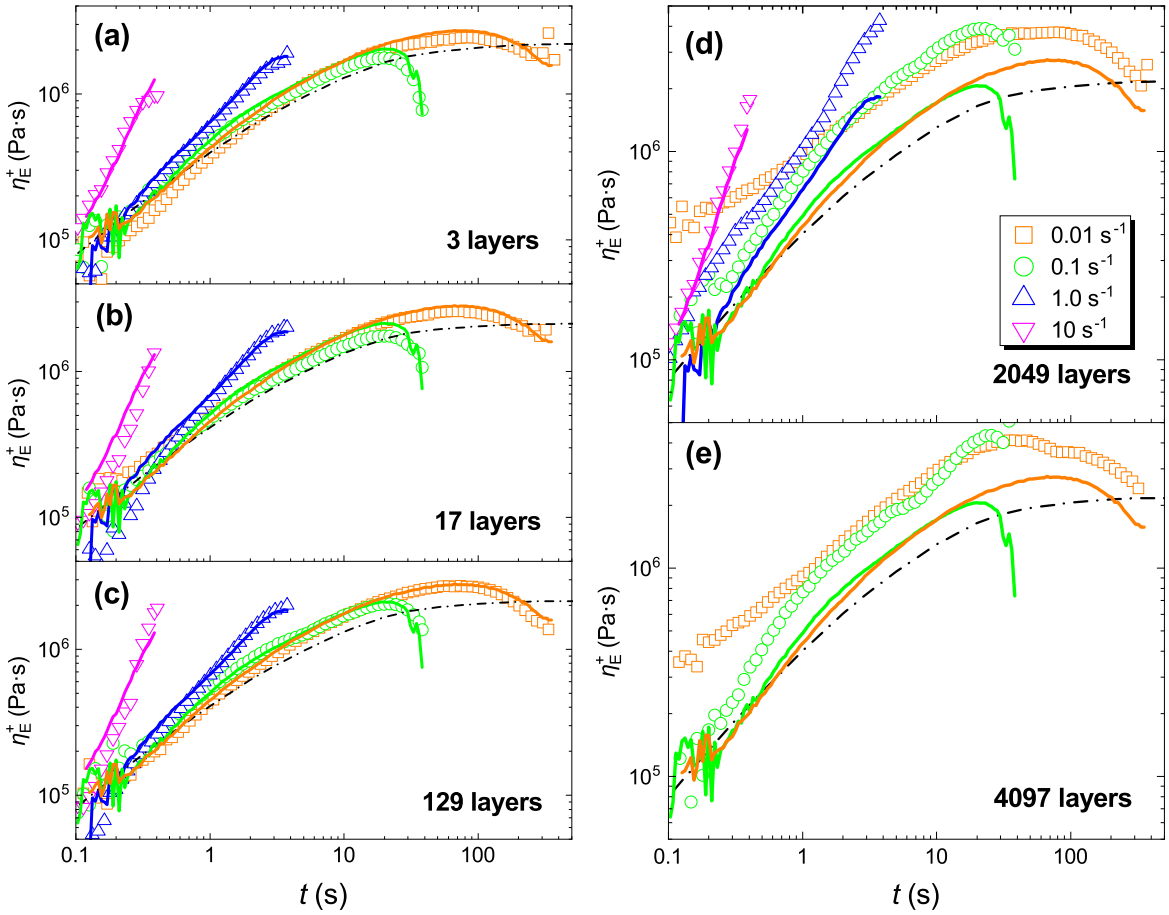

Figure S4: *Extensional viscosity of 30/70 PS/PMMA films with various number of layers: (a) 3; (b) 17; (c) 129; (d) 2049; (e) 4097 layers at various Hencky strain rates. The solid lines represent the additivity rule calculated from eq 4 for each strain rate, and the dashed lines are the theoretical LVE envelope. Note that the sample with 4097 layers was too thick to perform measurements at strain rates above 0.1* s^{-1}.

Extensional rheology calculations

The length (L), width (W), and thickness (H) of the sample change with experiment time and strain rate as follows[5]:

$$L(t) = L_0 \exp(\dot{\varepsilon} t) \tag{S2}$$

$$W(t) = W_0 \exp\left(\frac{-\dot{\varepsilon} t}{2}\right) \tag{S3}$$

$$H(t) = H_0 \exp\left(\frac{-\dot{\varepsilon} t}{2}\right) \tag{S4}$$

Melt volume ratio (ϕ) was defined to calculate the variation in thickness with the temperature change, including the density changes:

$$\phi = \left(\frac{H_{\mathrm{PS}}^{25^\circ\mathrm{C}}}{H_{\mathrm{PMMA}}^{25^\circ\mathrm{C}}}\right)\left(\frac{\rho_{\mathrm{PS}}^{25^\circ\mathrm{C}}}{\rho_{\mathrm{PS}}^{155^\circ\mathrm{C}}}\right)^{\frac{1}{3}}\left(\frac{\rho_{\mathrm{PMMA}}^{25^\circ\mathrm{C}}}{\rho_{\mathrm{PMMA}}^{155^\circ\mathrm{C}}}\right)^{-\frac{1}{3}} \tag{S5}$$

Since the density is difficult to measure at intermediate temperatures due to high viscosities, and because the variations for these polymers are small with temperature, we assume the density to follow a linear relation with temperature in the range of measured densities (Table S1) to estimate the one at 155 °C used in eq S5.

To verify the homogeneity of the layers in the films after the extensional rheometry measurements, two samples' cross-section areas were imaged by AFM after the tests and as close as possible to the breaking point. As seen in Figure S5, the layers remain continuous. Some broken layers were noted, as can be observed on the image of the sample with 2049 layers taken after the test with strain rate 10 s^{-1} but are rather due to processing instabilities than to the extensional experiment itself, as individual broken layers were already observed in some of the produced films (see the 'Film morphology' section of the manuscript).

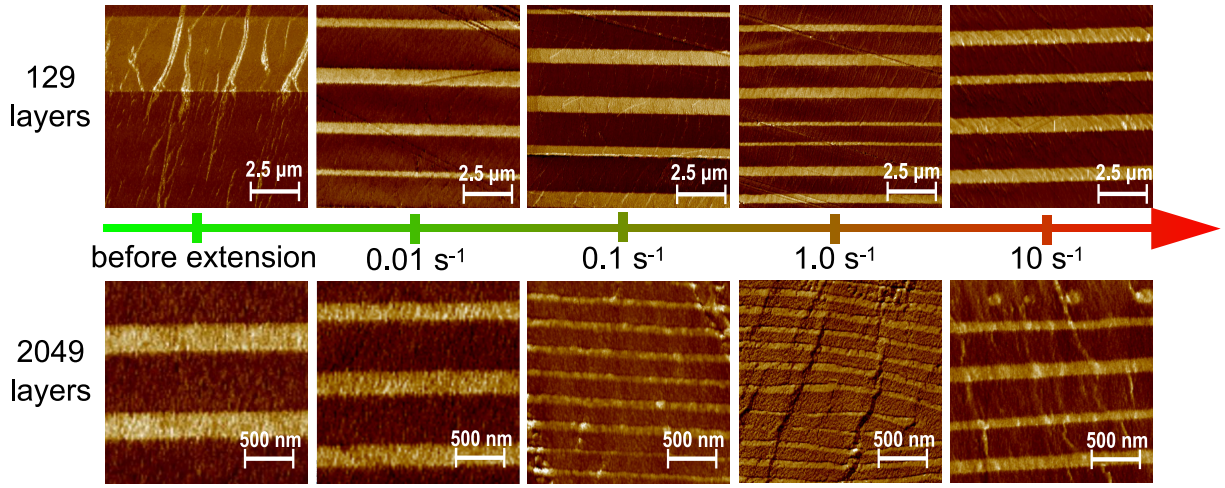

Figure S5: *AFM cross-sections of multilayer films after the extensional rheometry measurements until Hencky strain of 3.8, at increasing (from left to right) constant Hencky strain rates*

The exponential decay of the samples' cross-section area was also verified in our multilayer films. After performing interrupted tests with a strain rate 0.01 s^{-1} at 155 °C until strain equal to 0.8 and 1, the quenched samples were cut in the middle and imaged by AFM. As seen in Figure S6, the agreement between measured and calculated values (assuming exponential decay) of PS and PMMA layers' thicknesses is good.

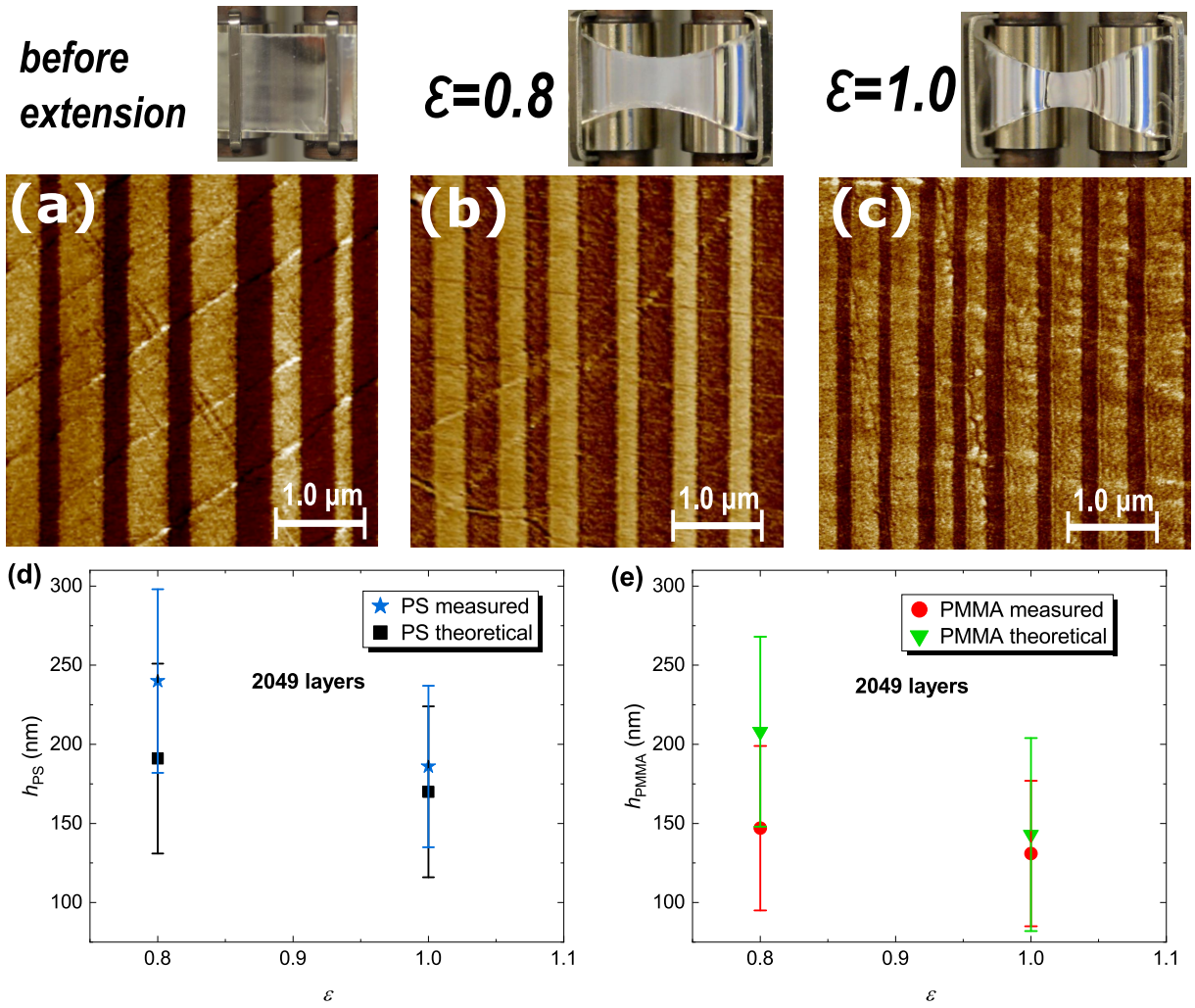

Figure S6: *Evidence of the exponential decrease of the layer thicknesses in the film with 2049 layers stretched with strain rate 0.01 s^{-1} at 155 °C. Pictures of the film on the SER accessory before extension, at strain 0.8 and 1 (top). AFM images of the cross-section of the films before extension (a) and at strain 0.8 (b) and 1 (c). Comparison of the theoretical versus measured thicknesses of PS (d) and PMMA (e) layers in the multilayer film.*

Interfacial contribution

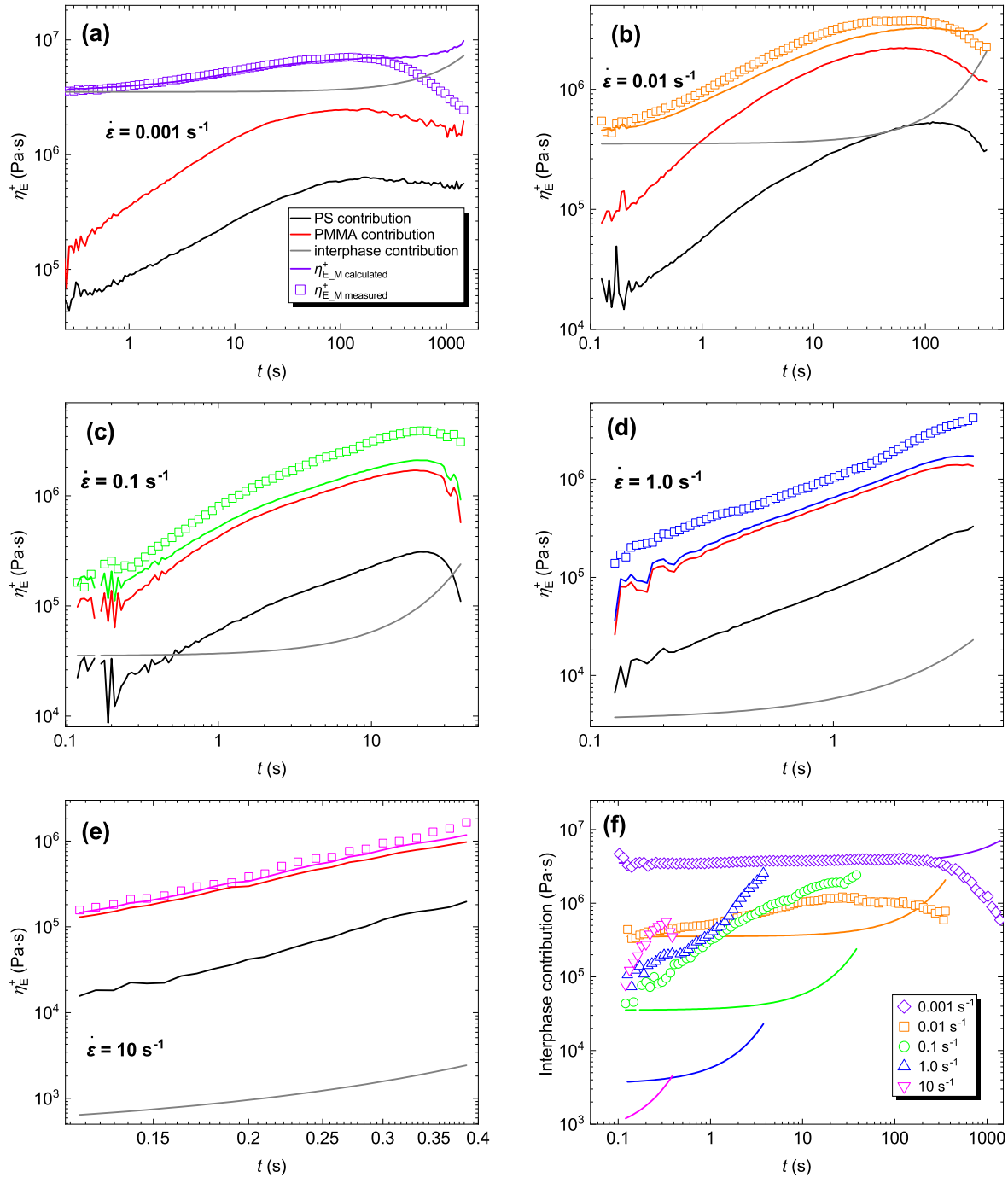

Figure S7: *Comparison between experimental data and additivity rule with the interfacial contribution for the 30/70 PS/PMMA film with 2049 layers. The color codes and organization of sub-figures are the same as in Figure 4.*

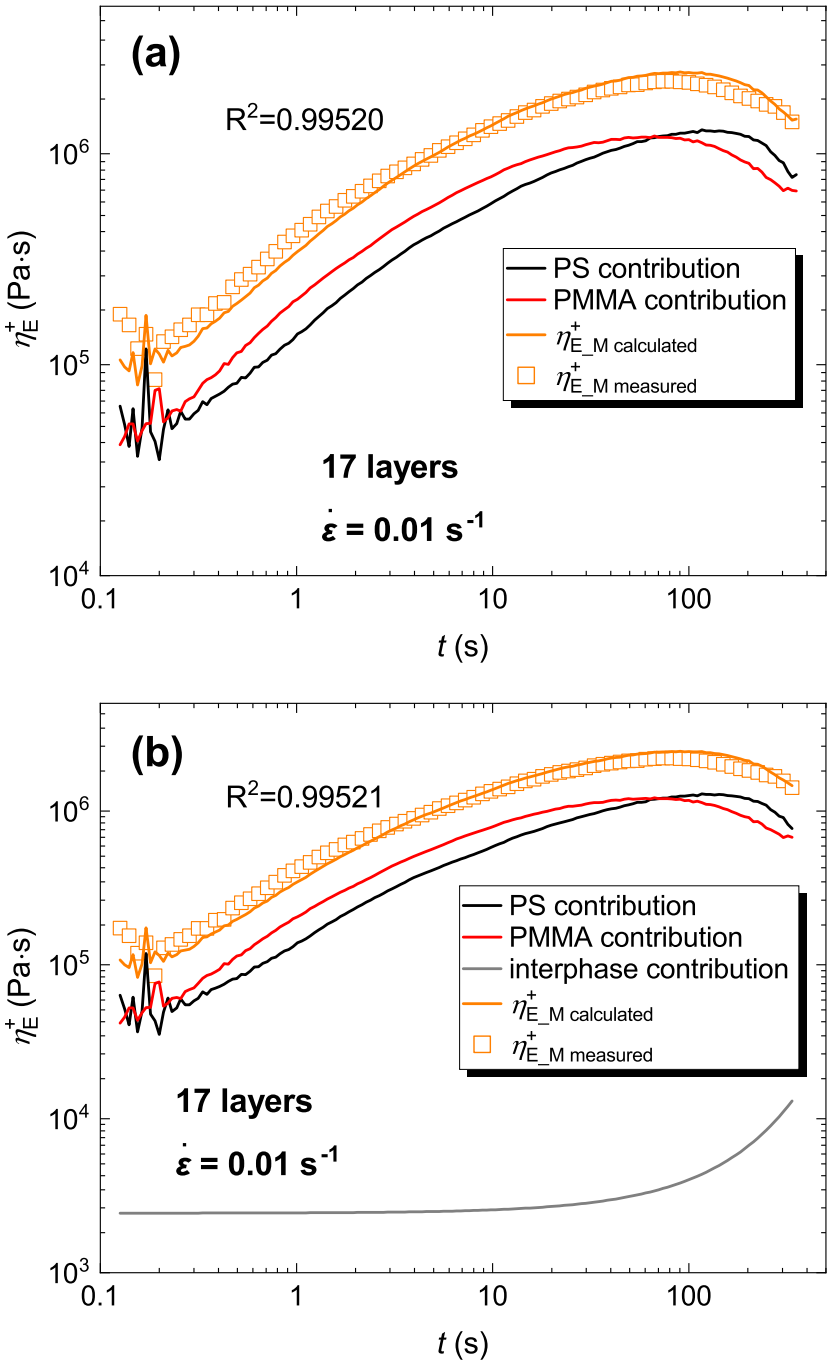

Figure S8: *Comparison between model without (a) and with (b) the interphase contribution for the 60/40 PS/PMMA film with 17 layers at strain rate 0.01* s^{-1}.

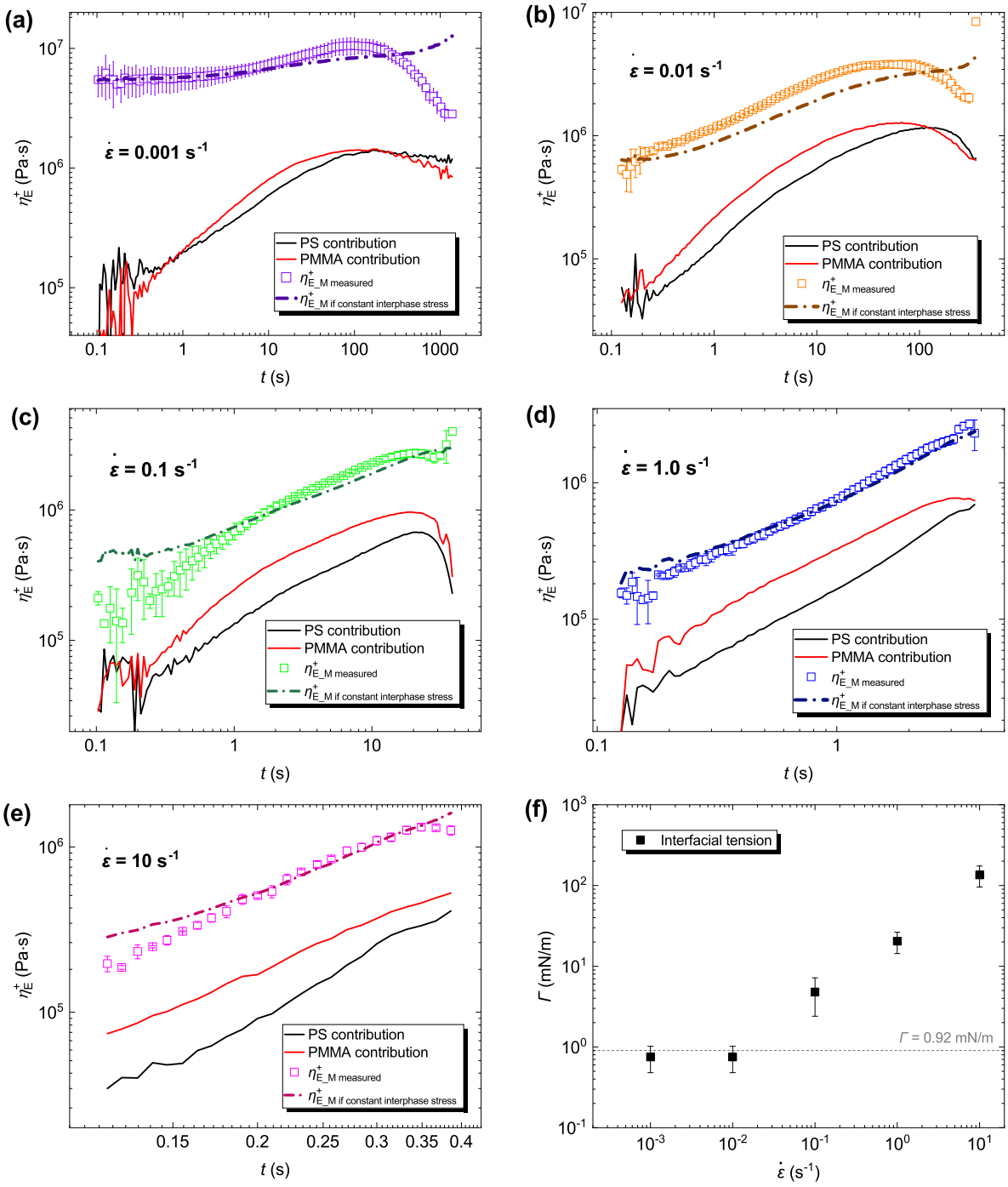

Figure S9: *Fits of the experimental data with interfacial tension as a free parameter following Jordan's approach (dashed-dotted lines) (a-e). Values of interfacial tension obtained from the fits (f).*

Interphase properties

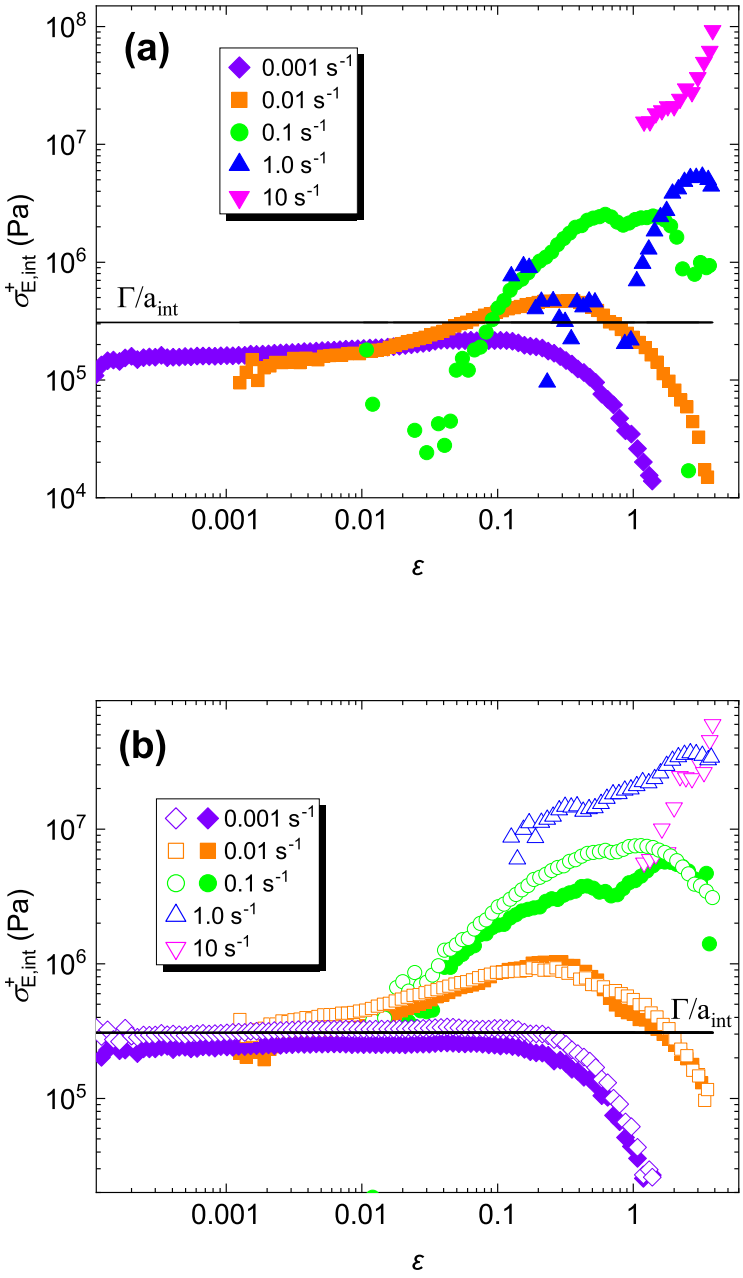

Figure S10: *Measured interphase stress as a function of strain. (a) composition 60/40 PS/PMMA, 4097 layers; (b) composition 30/70 PS/PMMA, 2049 layers (open symbols) and 4097 layers (closed symbols). The solid lines represent the equilibrium value from eq 8.*

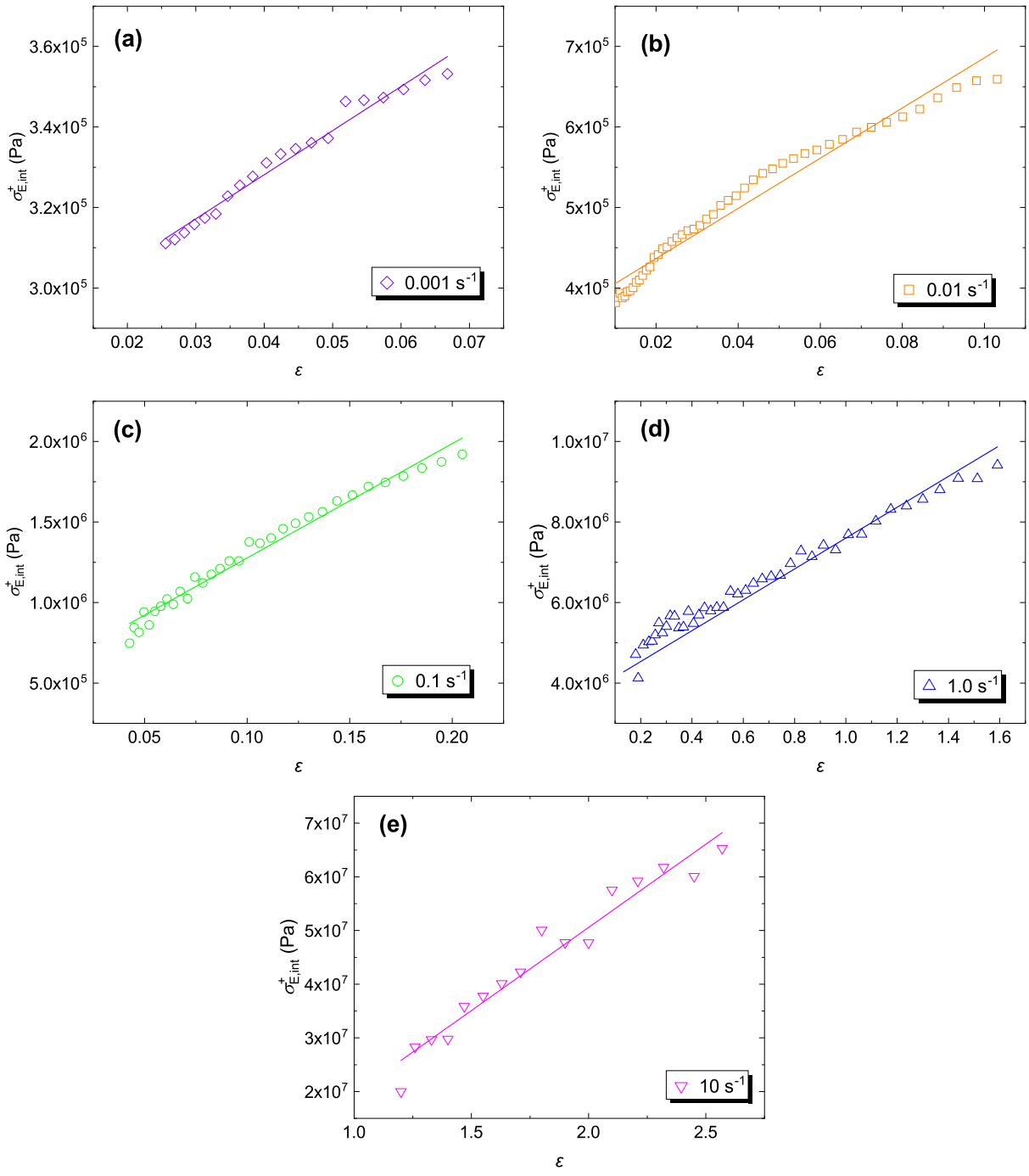

Figure S11: *The linear region of measured interphase stress as a function of strain for the same sample as in Figures 4 and 5, and at different strain rates: (a) 0.001 s^{-1}, (b) 0.01 s^{-1}, (c) 0.1 s^{-1}, (d) 1.0 s^{-1}, (e) 10 s^{-1}. The respective slopes represent the interphase moduli, $E_{\dot{\varepsilon}}$, which values are presented in Figure 6 (black squares).*

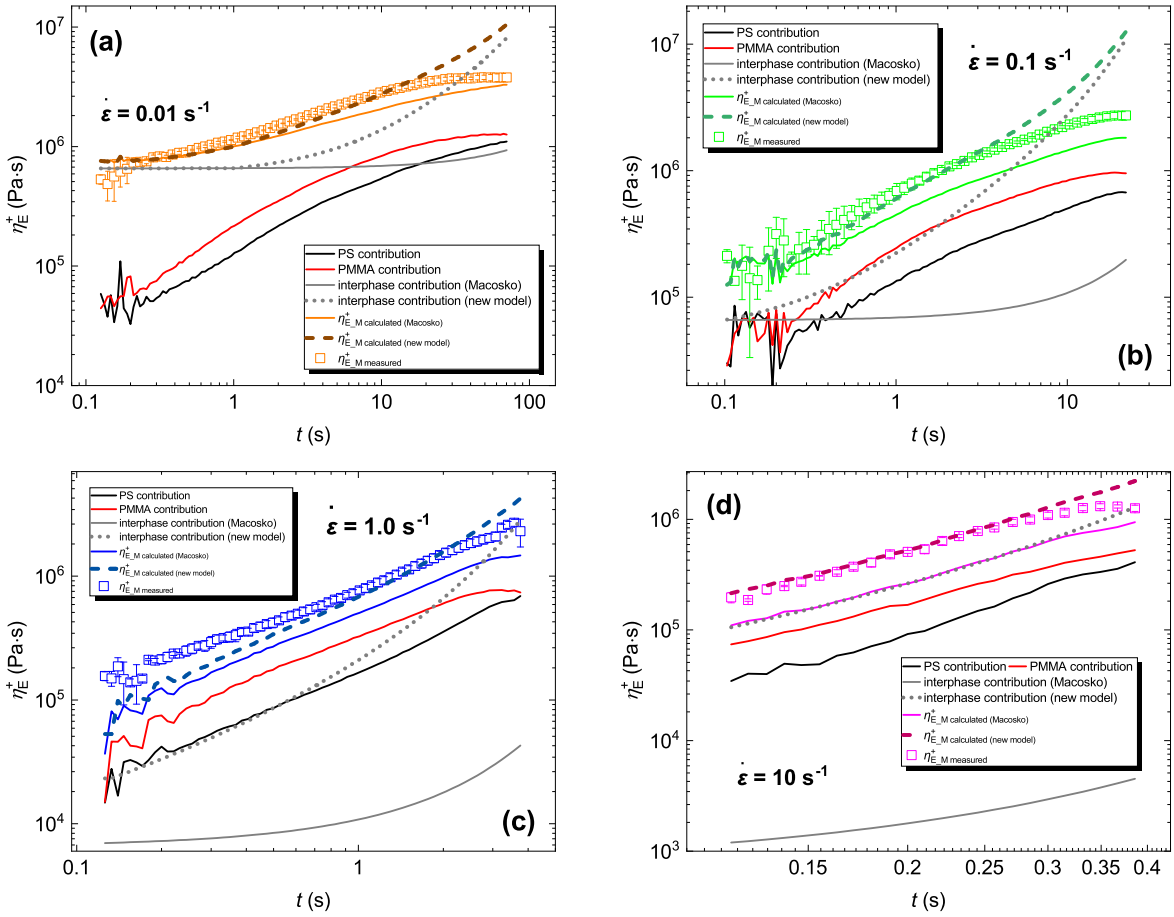

Figure S12: *Comparison of the experimental data with the model taking into account the interphase contribution and the interphase elasticity in the sample with 2049 layers and 60/40 PS/PMMA composition.*

References

(1) Zhu, Y.; Bironeau, A.; Restagno, F.; Sollogoub, C.; Miquelard-Garnier, G. Kinetics of thin polymer film rupture: Model experiments for a better understanding of layer breakups in the multilayer coextrusion process. *Polymer* **2016**, *90*, 156–164, DOI: 10.1016/j.polymer.2016.03.005.

(2) Bironeau, A.; Salez, T.; Miquelard-Garnier, G.; Sollogoub, C. Existence of a Critical Layer Thickness in PS/PMMA Nanolayered Films. *Macromolecules* **2017**, *50*, 4064–4073, DOI: 10.1021/acs.macromol.7b00176.

(3) Stamboulides, C.; Hatzikiriakos, S. G. Rheology and processing of molten poly (methyl methacrylate) resins. *Int. Polym. Process.* **2006**, *21*, 155–163, DOI: 10.3139/217.0081.

(4) Huang, Q.; Hengeller, L.; Alvarez, N. J.; Hassager, O. Bridging the gap between polymer melts and solutions in extensional rheology. *Macromolecules* **2015**, *48*, 4158–4163, DOI: 10.1021/acs.macromol.5b00849.

(5) Jordan, A. M.; Lee, B.; Kim, K.; Ludtke, E.; Lhost, O.; Jaffer, S. A.; Bates, F. S.; Macosko, C. W. Rheology of polymer multilayers: Slip in shear, hardening in extension. *J. Rheol.* **2019**, *63*, 751–761, DOI: 10.1122/1.5109788.

Supporting Information for 'Extensional Viscosity of Immiscible Polymers Multinanolayer Films: Signature of the Interphase'

Anna Dmochowska, Jorge Peixinho,* Cyrille Sollogoub, and Guillaume Miquelard-Garnier*

Laboratoire PIMM, CNRS, Arts et Métiers Institute of Technology, Cnam, HESAM Universite, 75013 Paris, France

E-mail: jorge.peixinho@cnrs.fr; guillaume.miquelardgarnier@lecnam.net

Characteristics of polymers used in the study

Table S1: *Properties of the polymers used in the study. The molar masses (M_W) and dispersities ($Đ$) were measured by Zhu et al.[1]; glass transition temperatures (T_g) were obtained from differential scanning calorimetry measurements on a Q10 analyzer (TA Instruments); the density at room temperature ($\rho_{25°C}$) was taken from the supplier technical sheet, and the density at 225 °C ($\rho_{225°C}$) was measured by Bironeau et al.[2]*

Polymer	M_W (kg/mol)	$Đ$	T_g (°C)	$\rho_{25°C}$ (g/cm^3)	$\rho_{225°C}$ (g/cm^3)
PS	245	2.2	96	1.05	0.95
PMMA	139	2.1	94	1.18	1.07

Viscoelastic properties of the neat polymer melts

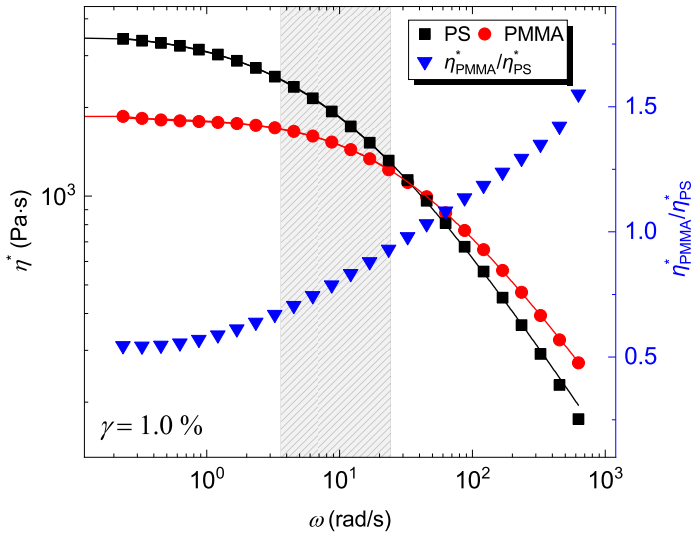

Figure S1: *Complex viscosity (η^*) of PS and PMMA as a function of angular frequency (ω) and their viscosity ratio at 225 °C and 1 % strain. The complex viscosity data were fitted with the Carreau-Yasuda model. The measurements were performed within the LVE region at shear strain 1 %. The gray area highlights the region corresponding to shear rate values found in our multilayer coextrusion setup when assuming the Cox-Merz rule.*[2]

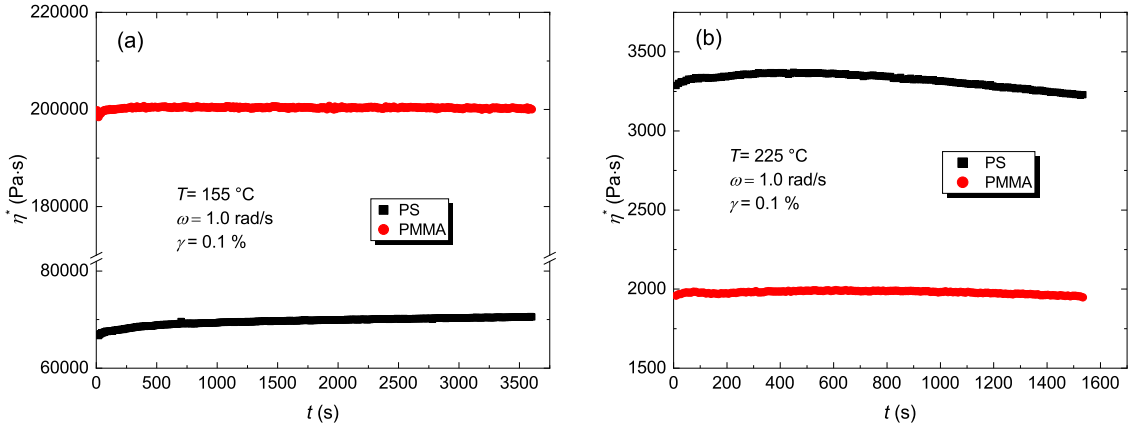

Figure S2: *Complex viscosity of PS and PMMA at 155 °C (a) and 225 °C (b) as a function of time. The measurements were performed within the LVE region at shear strain 0.1 % and with pulsation $\omega = 1$ rad/s. The maximum variation of viscosity values is 1.1 % for PS and 0.1 % for PMMA at 155 °C, and 4.5 % for PS and 0.5 % for PMMA at 225 °C, respectively.*

Characteristics of the fabricated PS/PMMA multilayer films

The theoretical thickness of the individual layer of each polymer can be calculated from the following equation:

$$h_{\mathrm{A}} = H_{\mathrm{M}} \times \frac{\phi_A}{n_A} \tag{S1}$$

where H_{M} is the total thickness of the multilayer film, ϕ_A is the volume fraction of polymer A in the film, and n_A the number of its layers. In the used coextrusion set-up, we start with the configuration A-B-A which in our case is PMMA-PS-PMMA. The number of layers n_A is calculated directly from the number of used LME with $n_A = 2^N + 1$. The equation is almost identical for polymer B (in our case PS) with $n_B = 2^N$.

Table S2: *Comparison of calculated and measured individual layer thicknesses.*

Fraction PS/PMMA (wt %)	Total no. of layers (n)	Film thickness (μm)	No. of measured layers	PS layer thickness		PMMA layer thickness	
				Calc. (nm)	Measured (nm)	Calc. (nm)	Measured (nm)
62/38	3	385 ± 39	3	186000	273700 ± 2300	83000	84500 ± 1400
60/40	17	587 ± 60	17	35200	453000 ± 5500	27800	27000 ± 2500
56/44	129	222 ± 20	30	1600	1800 ± 734	1400	1400 ± 570
57/43	2049	305 ± 16	240	131	159 ± 42	116	122 ± 29
56/44	2049	572 ± 45	220	298	287 ± 91	260	221 ± 78
53/47	4097	585 ± 87	425	115	124 ± 46	102	108 ± 34
53/47	4097	890 ± 72	438	232	198 ± 102	203	176 ± 77
29/71	3	607 ± 90	3	121000	192700 ± 12600	215000	237400 ± 7900
22/78	17	753 ± 39	17	19900	24000 ± 6600	70800	77200 ± 10300
19/81	129	799 ± 97	40	2800	2560 ± 700	9700	10440 ± 1700
25/75	2049	541 ± 37	240	106	132 ± 60	376	391 ± 91
26/74	4097	944 ± 47	425	90	111 ± 49	319	316 ± 104

Multimode Maxwell Model

Figure S3 reports the Time-Temperature superposition of SAOS data at reference temperature 155 °C of PS and PMMA together with the obtained fits of the 10-mode Maxwell model represented as lines. The relaxation moduli and time constants of the model are listed in Table S3. Note that the slope of G'' for PMMA at low reduced angular frequency is 1.7 rather than 2, as predicted by the Maxwell model, meaning we do not observe the terminal behavior[3]. The temperature behavior of both polymers is well captured by the WLF equation, in agreement with previous authors[4].

Table S3: *Linear Viscoelastic spectra for PS and PMMA at 155 °C.*

	PS		PMMA	
i	$\tau_i\,(s)$	$g_i\,(Pa)$	$\tau_i\,(s)$	$g_i\,(Pa)$
1	3.34×10^{0}	2.93×10^{4}	1.30×10^{0}	1.09×10^{5}
2	8.62×10^{-1}	4.14×10^{4}	1.94×10^{-1}	1.33×10^{5}
3	6.00×10^{-5}	1.74×10^{6}	2.73×10^{-3}	1.69×10^{5}
4	3.20×10^{-4}	4.00×10^{5}	3.90×10^{-5}	4.22×10^{6}
5	1.49×10^{-1}	5.25×10^{4}	1.05×10^{1}	4.54×10^{4}
6	1.35×10^{1}	1.93×10^{4}	3.80×10^{-5}	6.96×10^{5}
7	2.65×10^{-3}	1.88×10^{5}	2.74×10^{-3}	1.51×10^{5}
8	5.39×10^{-6}	2.30×10^{7}	2.60×10^{-2}	1.54×10^{5}
9	2.52×10^{-2}	5.37×10^{4}	4.50×10^{-4}	4.91×10^{5}
10	7.63×10^{1}	6.91×10^{3}	3.80×10^{-5}	2.68×10^{6}

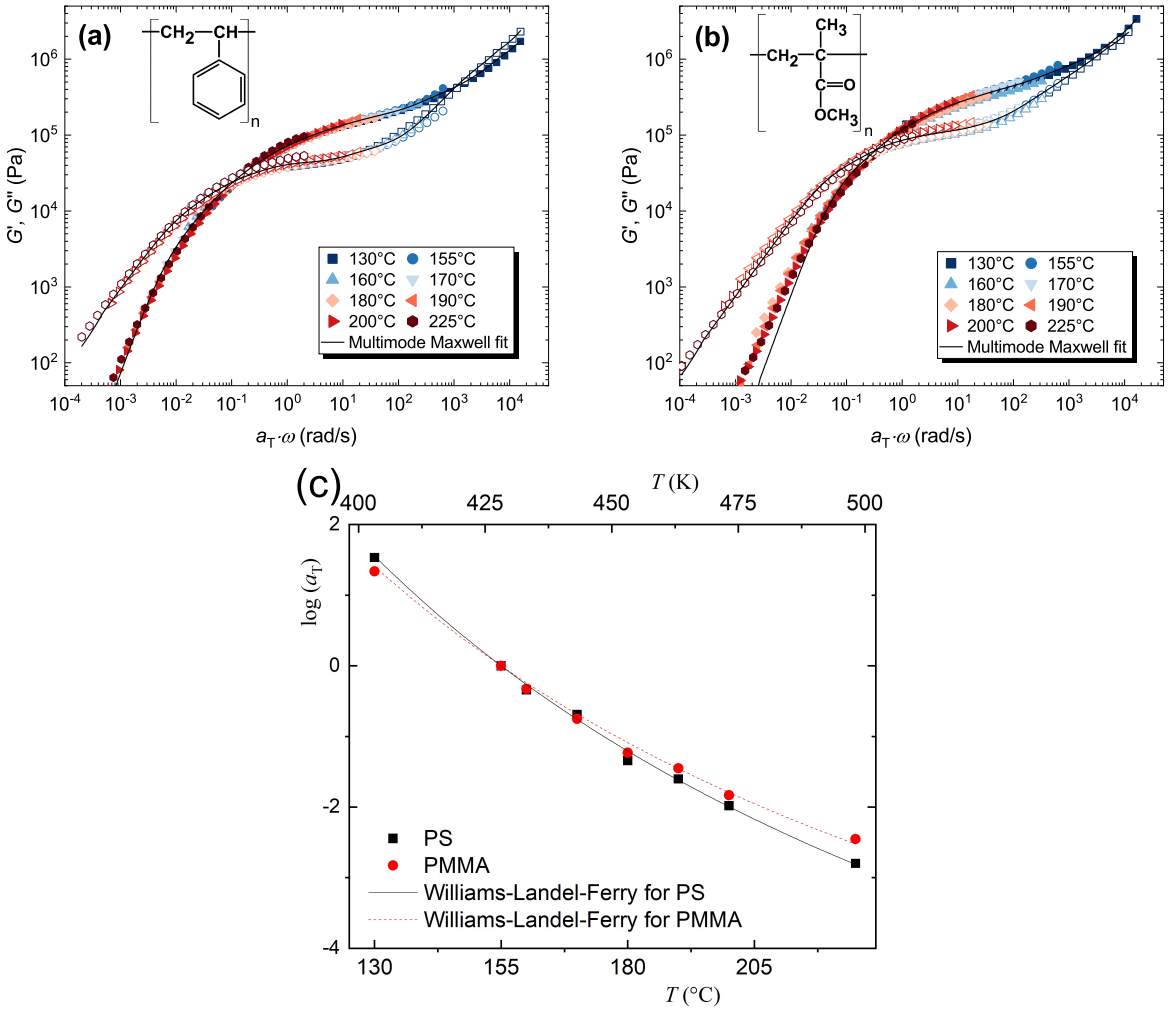

Figure S3: *Storage (G', open symbols) and loss (G'', closed symbols) moduli as a function of reduced angular frequency ($a_T\omega$) for PS (a) and PMMA (b). The superposition was done at $T_{ref} = 155$ °C. The lines represent the Maxwell fit described in the main body of the manuscript. (c) The shift factor, a_T, as a function of temperature. The lines represent the Williams-Landel-Ferry (WLF) equation: $\log a_T = -C_1 (T - T_{ref}) / (C_2 + T - T_{ref})$, where C_1 and C_2 are adjusted parameters.*

Extensional viscosity measurements

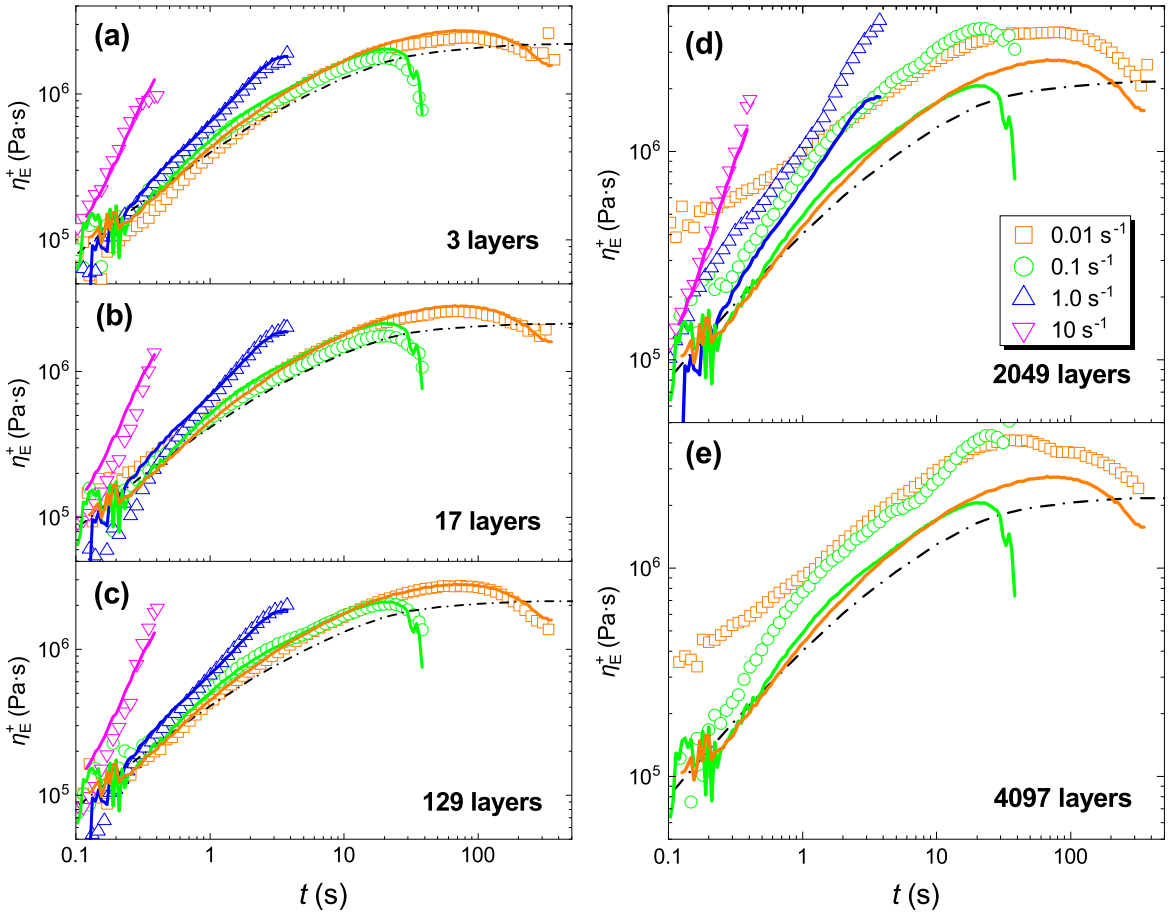

Figure S4: *Extensional viscosity of 30/70 PS/PMMA films with various number of layers: (a) 3; (b) 17; (c) 129; (d) 2049; (e) 4097 layers at various Hencky strain rates. The solid lines represent the additivity rule calculated from eq 4 for each strain rate, and the dashed lines are the theoretical LVE envelope. Note that the sample with 4097 layers was too thick to perform measurements at strain rates above 0.1* s^{-1}.

Extensional rheology calculations

The length (L), width (W), and thickness (H) of the sample change with experiment time and strain rate as follows[5]:

$$L(t) = L_0 \exp(\dot{\varepsilon} t) \tag{S2}$$

$$W(t) = W_0 \exp\left(\frac{-\dot{\varepsilon} t}{2}\right) \tag{S3}$$

$$H(t) = H_0 \exp\left(\frac{-\dot{\varepsilon} t}{2}\right) \tag{S4}$$

Melt volume ratio (ϕ) was defined to calculate the variation in thickness with the temperature change, including the density changes:

$$\phi = \left(\frac{H_{\mathrm{PS}}^{25^\circ\mathrm{C}}}{H_{\mathrm{PMMA}}^{25^\circ\mathrm{C}}}\right)\left(\frac{\rho_{\mathrm{PS}}^{25^\circ\mathrm{C}}}{\rho_{\mathrm{PS}}^{155^\circ\mathrm{C}}}\right)^{\frac{1}{3}}\left(\frac{\rho_{\mathrm{PMMA}}^{25^\circ\mathrm{C}}}{\rho_{\mathrm{PMMA}}^{155^\circ\mathrm{C}}}\right)^{-\frac{1}{3}} \tag{S5}$$

Since the density is difficult to measure at intermediate temperatures due to high viscosities, and because the variations for these polymers are small with temperature, we assume the density to follow a linear relation with temperature in the range of measured densities (Table S1) to estimate the one at 155 °C used in eq S5.

To verify the homogeneity of the layers in the films after the extensional rheometry measurements, two samples' cross-section areas were imaged by AFM after the tests and as close as possible to the breaking point. As seen in Figure S5, the layers remain continuous. Some broken layers were noted, as can be observed on the image of the sample with 2049 layers taken after the test with strain rate 10 s^{-1} but are rather due to processing instabilities than to the extensional experiment itself, as individual broken layers were already observed in some of the produced films (see the 'Film morphology' section of the manuscript).

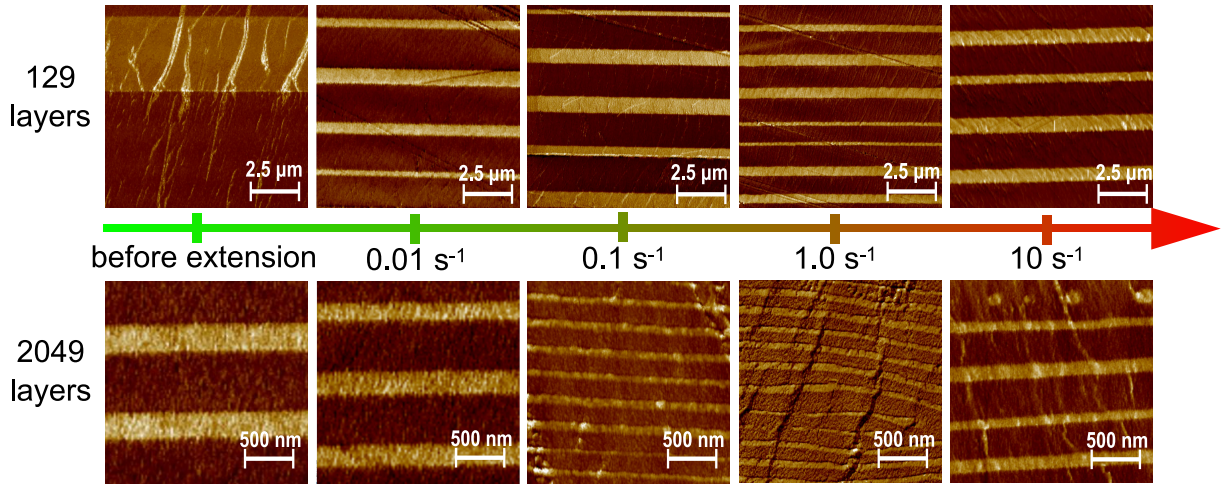

Figure S5: *AFM cross-sections of multilayer films after the extensional rheometry measurements until Hencky strain of 3.8, at increasing (from left to right) constant Hencky strain rates*

The exponential decay of the samples' cross-section area was also verified in our multilayer films. After performing interrupted tests with a strain rate 0.01 s^{-1} at 155 °C until strain equal to 0.8 and 1, the quenched samples were cut in the middle and imaged by AFM. As seen in Figure S6, the agreement between measured and calculated values (assuming exponential decay) of PS and PMMA layers' thicknesses is good.

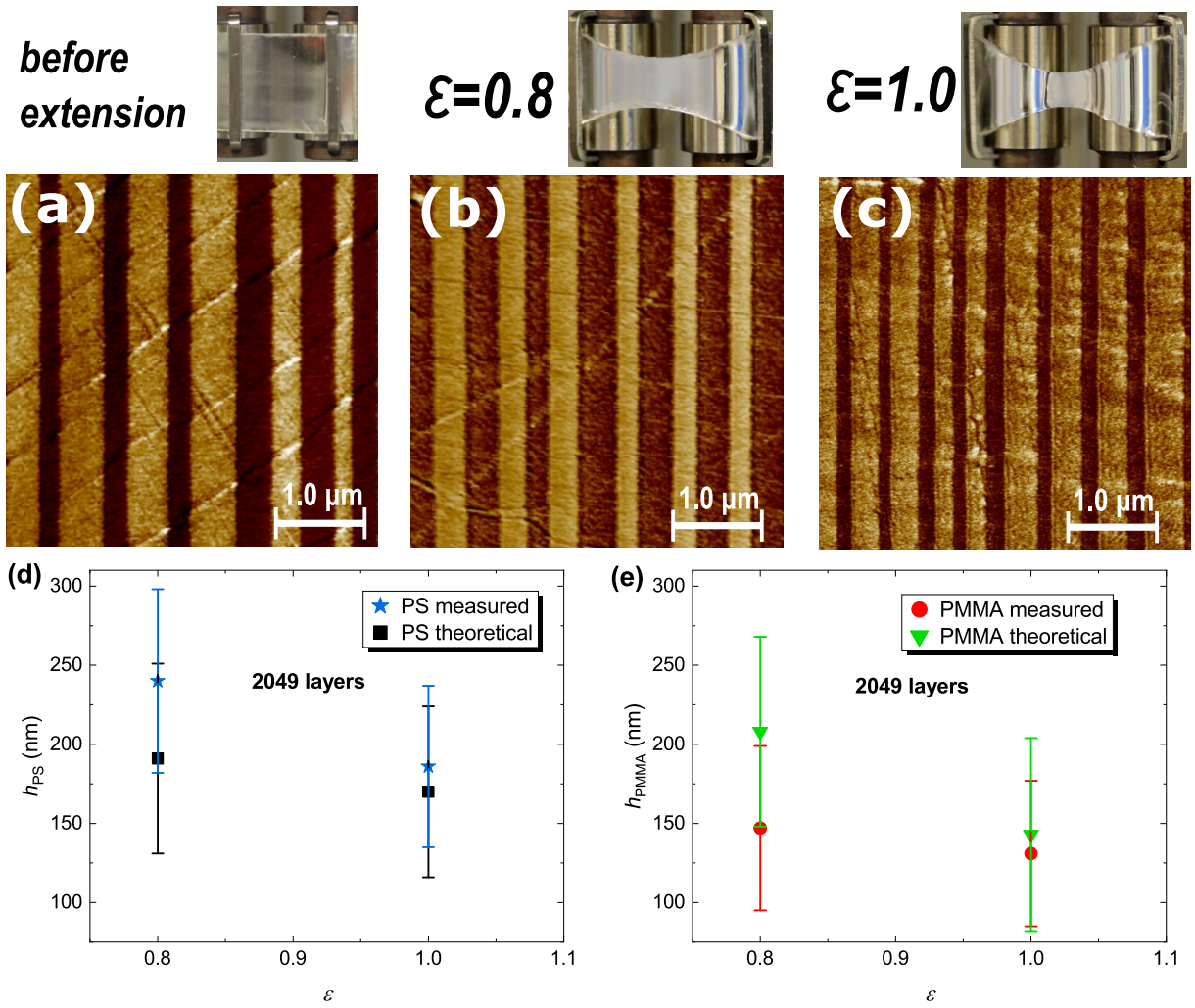

Figure S6: *Evidence of the exponential decrease of the layer thicknesses in the film with 2049 layers stretched with strain rate 0.01 s^{-1} at 155 °C. Pictures of the film on the SER accessory before extension, at strain 0.8 and 1 (top). AFM images of the cross-section of the films before extension (a) and at strain 0.8 (b) and 1 (c). Comparison of the theoretical versus measured thicknesses of PS (d) and PMMA (e) layers in the multilayer film.*

Interfacial contribution

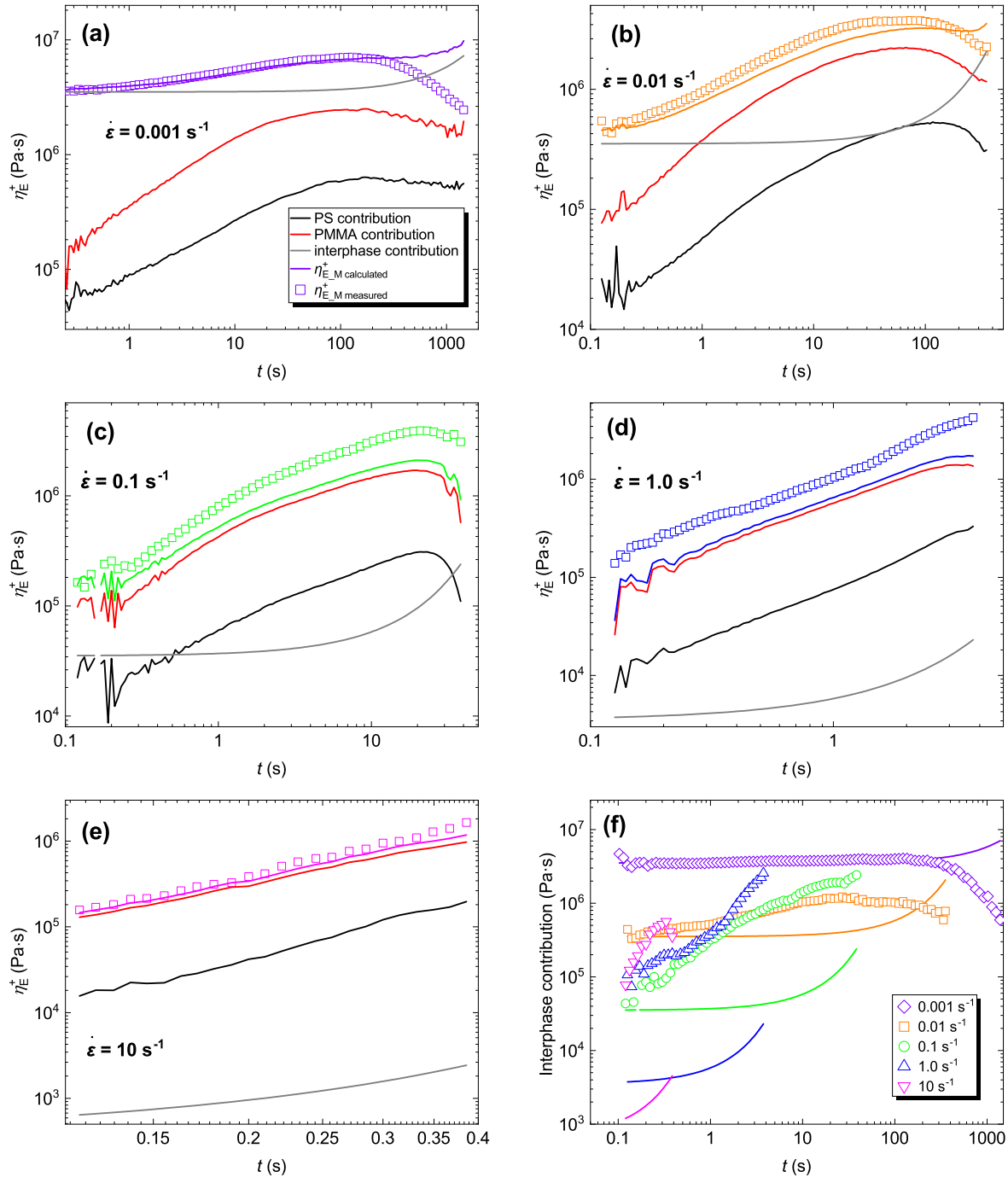

Figure S7: *Comparison between experimental data and additivity rule with the interfacial contribution for the 30/70 PS/PMMA film with 2049 layers. The color codes and organization of sub-figures are the same as in Figure 4.*

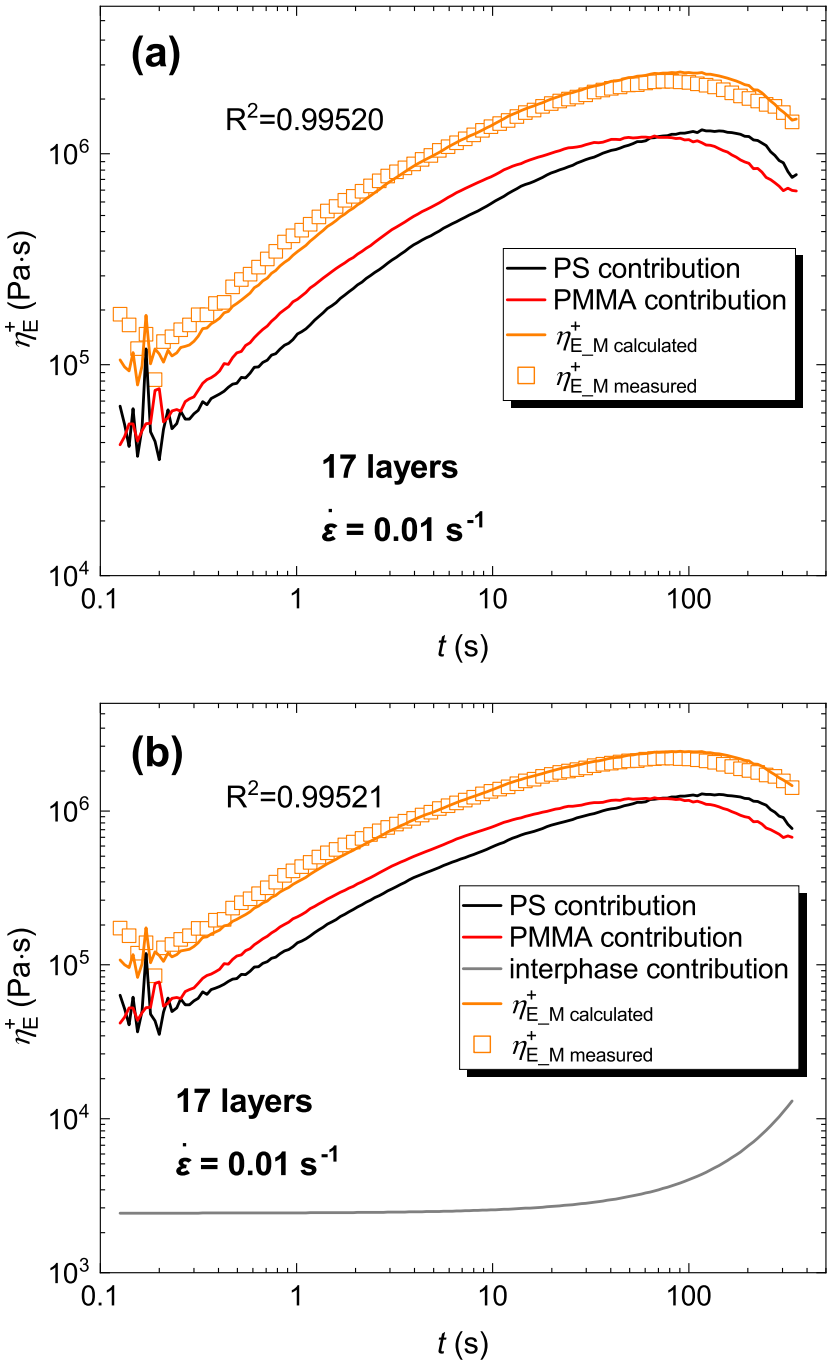

Figure S8: *Comparison between model without (a) and with (b) the interphase contribution for the 60/40 PS/PMMA film with 17 layers at strain rate 0.01* s^{-1}.

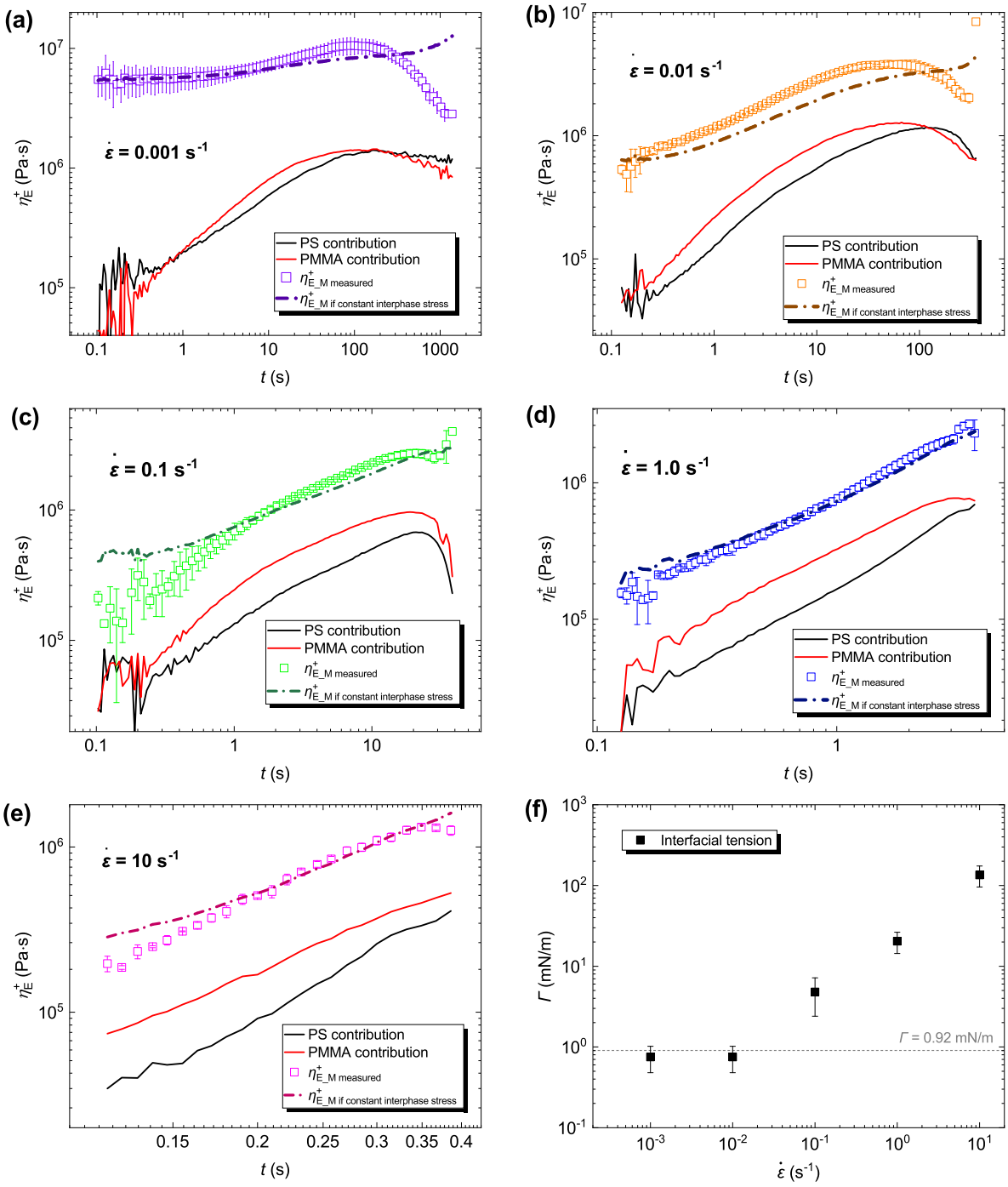

Figure S9: *Fits of the experimental data with interfacial tension as a free parameter following Jordan's approach (dashed-dotted lines) (a-e). Values of interfacial tension obtained from the fits (f).*

Interphase properties

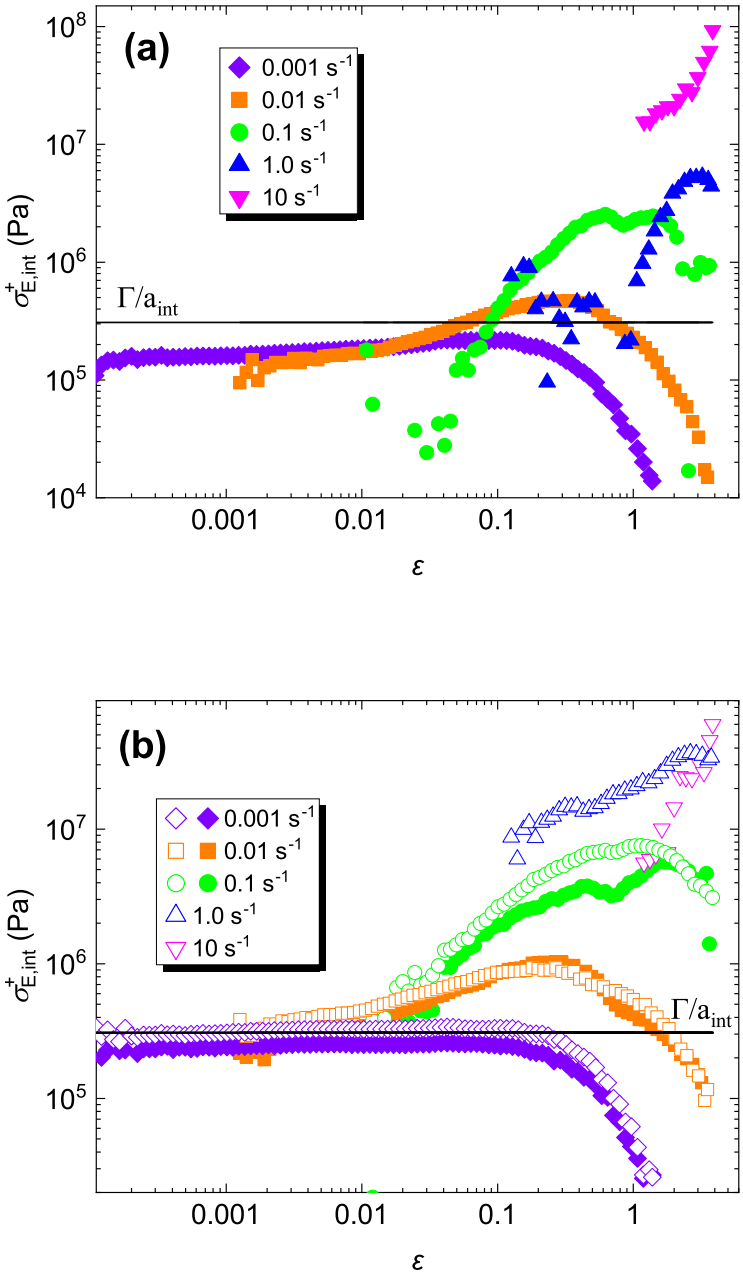

Figure S10: *Measured interphase stress as a function of strain. (a) composition 60/40 PS/PMMA, 4097 layers; (b) composition 30/70 PS/PMMA, 2049 layers (open symbols) and 4097 layers (closed symbols). The solid lines represent the equilibrium value from eq 8.*

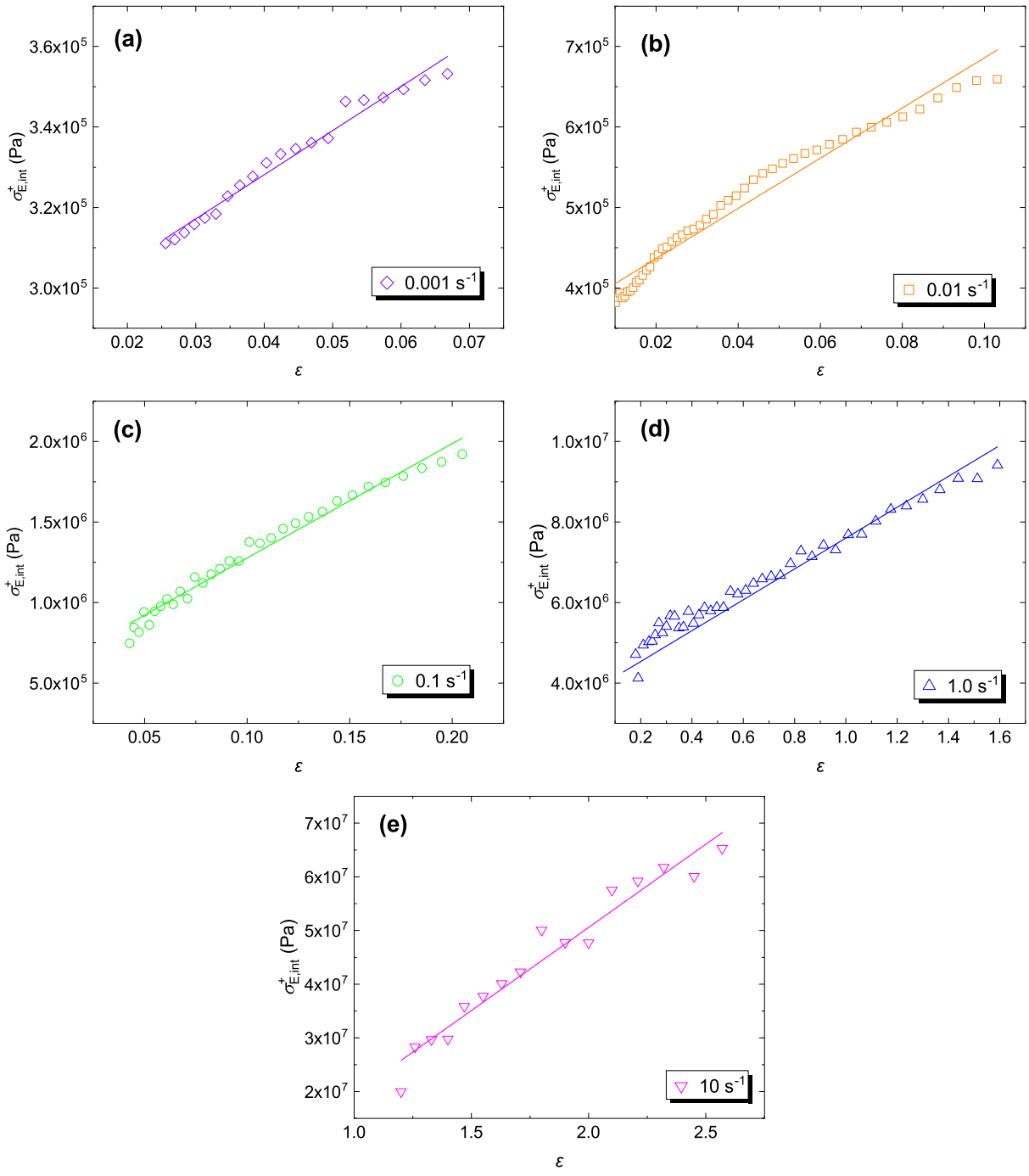

Figure S11: *The linear region of measured interphase stress as a function of strain for the same sample as in Figures 4 and 5, and at different strain rates: (a) 0.001 s^{-1}, (b) 0.01 s^{-1}, (c) 0.1 s^{-1}, (d) 1.0 s^{-1}, (e) 10 s^{-1}. The respective slopes represent the interphase moduli, $E_{\dot{\varepsilon}}$, which values are presented in Figure 6 (black squares).*

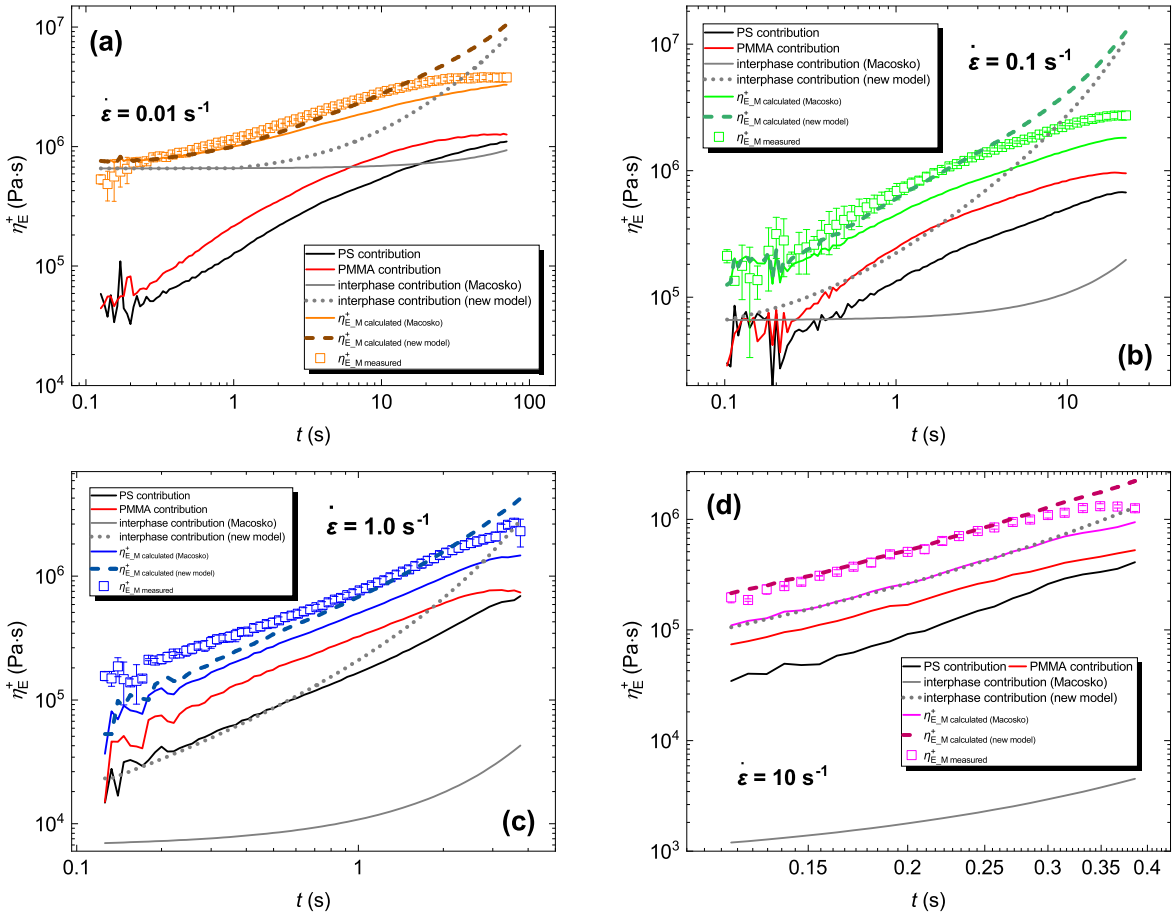

Figure S12: *Comparison of the experimental data with the model taking into account the interphase contribution and the interphase elasticity in the sample with 2049 layers and 60/40 PS/PMMA composition.*

References

(1) Zhu, Y.; Bironeau, A.; Restagno, F.; Sollogoub, C.; Miquelard-Garnier, G. Kinetics of thin polymer film rupture: Model experiments for a better understanding of layer breakups in the multilayer coextrusion process. *Polymer* **2016**, *90*, 156–164, DOI: 10.1016/j.polymer.2016.03.005.

(2) Bironeau, A.; Salez, T.; Miquelard-Garnier, G.; Sollogoub, C. Existence of a Critical Layer Thickness in PS/PMMA Nanolayered Films. *Macromolecules* **2017**, *50*, 4064–4073, DOI: 10.1021/acs.macromol.7b00176.

(3) Stamboulides, C.; Hatzikiriakos, S. G. Rheology and processing of molten poly (methyl methacrylate) resins. *Int. Polym. Process.* **2006**, *21*, 155–163, DOI: 10.3139/217.0081.

(4) Huang, Q.; Hengeller, L.; Alvarez, N. J.; Hassager, O. Bridging the gap between polymer melts and solutions in extensional rheology. *Macromolecules* **2015**, *48*, 4158–4163, DOI: 10.1021/acs.macromol.5b00849.

(5) Jordan, A. M.; Lee, B.; Kim, K.; Ludtke, E.; Lhost, O.; Jaffer, S. A.; Bates, F. S.; Macosko, C. W. Rheology of polymer multilayers: Slip in shear, hardening in extension. *J. Rheol.* **2019**, *63*, 751–761, DOI: 10.1122/1.5109788.